RESONANCE IONIZATION SPECTROSCOPY FOR THE ULTRATRACE DETECTION OF MERCURY

By

WENDY LEIGH CLEVENGER

A DISSERTATION PRESENTED TO THE GRADUATE SCHOOL
OF THE UNIVERSITY OF FLORIDA IN PARTIAL FULFILLMENT
OF THE REQUIREMENTS FOR THE DEGREE OF
DOCTOR OF PHILOSOPHY

UNIVERSITY OF FLORIDA

1997

This dissertation is dedicated to the memory of my grandfather Charles Anderson Clevenger and my grandmother Agnes Creasman Wooten Garner

ACKNOWLEDGMENTS

I have often thought about all of the things I could have done with the past four years of my life traveling, spending time with family and friends, taking it easy and smelling the roses Now that I see the light at the end of the graduate school tunnel I can fully realize and appreciate the experiences I have had as a graduate student

The main thanks for getting me through any of this go to Dr James Winefordner His awe-inspiring enthusiasm, knowledge, and laughter have set an example that I hope to carry with me always His understanding and respect for his students are something to be cherished and has made me realize how lucky I am to have been in his group

Equal thanks go to Dr Benjamin Smith for his friendship and constant support His vision of what good science is has always inspired me to excel and shine in ways I wasn t sure I could

Further gratitude is extended to Drs. Oleg Matveev and Nicolo Omenetto, with whom I have been fortunate enough to be associated with for the past two years. Oleg s enthusiasm and creativity and Nico s love of his work and those sharing in it have shown me what characteristics I would like to have as a scientist. I must also thank Leah Morton Rater Susana Cabredo and Qing Sun for their assistance in this work.

In addition I would like to thank Dr Kathryn Williams for her support and advice and for giving me an example of how hard work for students can pay off. I must also

thank Dr Robert Kennedy Dr Joseph Delfino Dr Jim Dayrup and Dr Rick Yost for their help and support, as well as the US National Institutes of Health, the US Department of Energy and especially the US Environmental Protection Agency for their help in funding this work.

Most importantly, I must thank my parents Jerry and Linda Clevenger, for the love, support, and encouragement I have been lucky enough to receive my whole life. Their never waning faith in me and my abilities are what have gotten me where I are today I am also grateful to my brother Chuck and sister Christy as well as the rest of my family I feel most blessed to have all of them and the knowledge that they are always there for me

I must also thank the friends that I have made, from whom I have gained much support over the past four years. These include JDW group members Rob Guenard, Dave Rusak, Arthur Besteman, Scott Baker, Andrea Crosbyn, Bryan Castle, and Berky Litteral Equally important are Tracie Williams, Eve Hinovice, Sunday Brooks, Brendan Boyd, Mike Bruner, Aaron Williams, Scott Gordon and Yannis Karayannis. I also give many thanks to Angie Schuelke for her support and friendship over the past ten years.

Thank you God for all of the wonderful opportunities and experiences you have given me

TABLE OF CONTENTS

page

ACKNOWLEDGMENTS ... iii

LIST OF TABLES ... viii

ABSTRACT ... ix

CHAPTER 1 THE GOAL OF THE PROJECT ... 1

CHAPTER 2 SPECTROSCOPIC TECHNIQUES FOR THE TRACE DETECTION OF MERCURY ... 3
Previous Reviews ... 3
Sample Introduction ... 4
Cold Vapor Atomic Absorption Spectrometry ... 6
No Preconcentration ... 6
Preconcentration ... 9
Flame Atomic Absorption Spectrometry ... 14
Electrothermal Atomization Atomic Absorption Spectrometry ... 14
Speciation Coupled with Atomic Absorption Spectrometry ... 15
Flame Atomic Fluorescence Spectrometry ... 17
Cold Vapor Atomic Fluorescence Spectrometry ... 17
No Preconcentration ... 17
Preconcentration ... 19
Electrothermal Atomization Laser Enhanced Atomic Fluorescence Spectrometry ... 20
Inductively Coupled Plasma Atomic Fluorescence Spectrometry ... 20
Speciation Coupled with Atomic Fluorescence Spectrometry ... 21
Microwave Induced Plasma Atomic Emission Spectrometry ... 22
Inductively Coupled Plasma Atomic Emission Spectrometry ... 23
DC Discharge Plasma Atomic Emission Spectrometry ... 25
Ring Discharge Plasma Atomic Emission Spectrometry ... 25
Speciation Coupled with Atomic Emission Spectrometry ... 25
Photoacoustic Spectrometry ... 27
Metastable Energy Transfer for Atomic Luminescence ... 27
Magnetically-Induced Optical Rotation ... 28
X-Ray Fluorescence Spectrometry ... 28

^{199}Hg Nuclear Magnetic Resonance Spectrometry 28
Laser Induced Breakdown Spectrometry 28
Furnace Atomic Non-Thermal Excitation Spectrometry 29
Inductively Coupled Plasma Mass Spectrometry 30
No Preconcentration 31
Preconcentration 31
Speciation Coupled with Inductively Coupled Plasma Spectrometry 31
Spectrophotometry 31
Fluorimetry 34
Summary of Techniques 35
Resonance Ionization Spectroscopy 36
Principles 36
Resonance Ionization Spectroscopy of Mercury 39

CHAPTER 3 ANALYTICAL TIME-RESOLVED RESONANCE IONIZATION SPECTROSCOPY 41

Experimental 43
Results and Discussion 49
DensMat Simulations 49
Excitation of Levels n = 10-14 52
Excitation of Levels n = 18-21 54
Signal vs. Pressure 56
Signal vs. Beam Position Between Electrodes 62
Signal vs. Laser Power 62
Conclusions 67

CHAPTER 4 RESONANCE IONIZATION SPECTROSCOPY OF MERCURY RYDBERG STATES 69

Experimental 72
Results and Discussion 76
Assigning Spectral Lines 76
Stark Effects 78
Buffer Gas Pressure Shifts and Broadenings 84
Conclusions 89

CHAPTER 5 RESONANCE IONIZATION OF MERCURY ATOMS IN AN INERT ATMOSPHERE WITH AVALANCHE AMPLIFICATION OF THE SIGNAL 91

Experimental 93
Results and Discussion 98
Signal vs. Temperature 98
Avalanche Amplification 102
Limit of Detection 106

Conclusions 118

CHAPTER 6 METHOD OPTIMIZATION AND ANALYTICAL CONSIDERATIONS 119

Experimental 119
Results and Discussion 122
Performance of Excitation Scheme 122
Performance of Electron Counter 124
Limit of Detection 126
Analytical Curve 130
Conclusions 132

CHAPTER 7 FUTURE WORK 134

LIST OF REFERENCES 136

BIOGRAPHICAL SKETCH 146

LIST OF TABLES

Table page

3-1 Excitation transitions for Hg for laser-connected levels 1,2,3, and 4 (Rydberg level), as tabulated by Moore for $n = 6, 7, 9$-26 45

4-1 Excitation transitions for Hg for laser-connected levels 1,2,3 and 4 (Rydberg level), as tabulated by Moore, Baig, and in this work for $n = 6, 7,$ 10-48 73-5

5-1 Excitation transitions for Hg for laser-connected levels 1 2,3 and 4 (Rydberg level) as tabulated by Moore for $n = 6, 7, 9$-13 95

Abstract of Dissertation Presented to the Graduate School
of the University of Florida in Partial Fulfillment of the
Requirements for the Degree of Doctor of Philosophy

RESONANCE IONIZATION SPECTROSCOPY FOR THE ULTRATRACE DETECTION OF MERCURY

By

Wendy Leigh Clevenger

August 1997

Chairman: James D. Winefordner
Major Department: Chemistry

Resonance ionization spectroscopy (RIS) has been proven to be one of the most sensitive and selective methods for trace metal detection available today. This sensitivity can be further improved when an inert atmosphere can be used as the sample introduction method (i.e., a stream of inert gas) instead of a flame or furnace. For these reasons, it is an ideal method for detection of mercury in environmental samples in combination with the well-established method of cold vapor generation of mercury atoms from solution.

RIS involves the stepwise excitation of the mercury atom to a state near the ionization continuum. From here, ionization of the atom occurs and the resultant electrons are detected as an electrical current. In this work, three dye lasers pumped by an excimer laser were used to excite the atoms. The detection occurs in a quartz cell or

novel electron counter into which the mercury atoms were swept by a stream of buffer gas. A high voltage (0 - 3.5 kV) was applied between two electrodes to allow collection of the electrons. The signal was amplified and recorded on a digitizing oscilloscope and laptop computer.

Fundamental studies of mercury Rydberg states were carried out in order to find the optimal conditions for ultratrace detection. These studies included the effect of the choice of gas pressure and applied high voltage on the spectral lines. In addition, the use of avalanche amplification of the electrical signal was investigated and determined to give a signal 6.6 x 10^3 times higher than the signal observed with the normal RIS setup. With this increase in signal, a limit of detection of 15 atoms is calculated. The limit of detection experimentally determined is 1.9 x 10^5 atoms in the measurement volume, which was limited by poor ionization efficiency. A preliminary study involving the generation of mercury by the cold vapor method from aqueous standards, using an unoptimized RIS detection scheme and sample introduction apparatus, showed linearity with mercury amounts over a wide range.

CHAPTER 1
THE GOAL OF THE PROJECT

The contamination of the environment by mercury has been an important concern throughout the world for decades. Mercury as a liquid with a high thermal conductivity has many unique properties which make it useful in more than three thousand industrial applications ranging from fungicides and bactericides in the agriculture industry to heat transfer agents and catalysts in the chemical industry. At the same time, mercury is a highly toxic element that can cause kidney injury, central nervous system disorders, intellectual deterioration, and even death. The tragic effects of unrestricted industrial mercury dumping became undeniable in the mid-1950s, when more than a hundred people in Minimata, Japan died from eating fish contaminated by a methyl mercury discharge. After this disaster industrialized nations around the world began prohibiting the dumping of mercury into waterways. This decrease of anthropogenic sources resulted in falling levels of mercury compounds in lakes and rivers that had been receiving these discharges.

Nevertheless, mercury contamination remains an important environmental problem in the 1990s. Mercury poisoning of both the environment and the human race is currently observed not only in unregulated areas such as the Brazilian Amazon[1,2] but also in the United States Great Lakes region[3,4] and the Florida Everglades.[5,6] Sources range from unrestricted dumping to atmospheric deposition and agricultural runoff. Clearly the

problem of mercury is not going away and thus the need for analytical techniques capable of detecting trace amounts of mercury is still of importance. Also, as environmental levels of mercury are reduced, increasingly sensitive techniques are required to monitor its distribution.

The goal of this work was to create a method for the detection of mercury at ultratrace (ppb and less) levels. This method involved the use of resonance ionization spectroscopy (RIS), one of the most sensitive and selective methods for trace metal detection available today. Fundamental studies of the RIS of Hg were carried out to find the optimal conditions for this method. In addition, studies involving the avalanche amplification of the signal were carried out to optimize this method of signal enhancement. Final studies involved attempts to improve the limit of detection and studies of the linearity of the signal with concentration in order to prove this method as an analytically useful technique for ultratrace detection. Mercury was detected in the gas phase from ambient air as well as from aqueous samples using the technique of cold vapor generation of Hg atoms from solution into the gas phase.

CHAPTER 2
SPECTROSCOPIC TECHNIQUES FOR THE TRACE DETECTION OF MERCURY

Previous Reviews

The early history of mercury detection was given by Woodson[7] in one of the first papers on the cold vapor atomic absorption detection of mercury, published in 1939. This short review was limited to the then-dominant colorimetric techniques and early optical methods. A 1975 review by Chilov[8] discussed techniques for determining mercury at the ppm level or less with 339 references, most of which were published after 1965. It covered sampling and sample storage as well as methods of analysis, with an emphasis on sensitivity and ease of application. This report acknowledged the replacement of colorimetry[9] by atomic absorption as the generally accepted technique, while noting that neutron activation allowed non-destructive analysis. An appendix listing the different techniques with their lower useful limits in different sample types was given. Another 1975 review by Ure[10] covered non-flame atomic absorption and fluorescence spectrometry determination of mercury. Non-flame methods here include pyrolysis, furnace techniques, combustion, and reduction-aeration (cold vapor) methods of sample introduction. However, while these non flame methods were simple and sensitive, they experienced difficulties in giving accurate determinations in natural samples. Four

hundred forty-two references were given In addition, they were catalogued by application

In 1995 Morita, Tanaka, and Shimomura[11] reviewed atomic fluorescence spectrometry (AFS) methods for determining mercury They noted that at that time cold vapor (CV) AFS and CV atomic absorption spectrometry (AAS) were the most widely used methods for determining Hg. The review discussed the principles of AFS of Hg, the use of flow injection (FI) techniques, and applications of CV-AFS Ninety-one references were given

Sample Introduction

The most convenient and widely used method of sample introduction of mercury is the cold vapor technique, because mercury has a vapor pressure of 0 16 Pa at 20° C corresponding to a concentration of ~14 mg m^{-3} in air The cold vapor technique allows direct determination without an atomizer unit. Liquid samples can be analyzed by reducing the Hg ions in solution and aerating inert gas through the liquid to liberate all elemental Hg into the gas phase Similarly, solid samples (soil, tissue, etc) can be digested and the solution reduced and aerated

Other flameless techniques still in use include furnace techniques, both with and without *in situ* preconcentration, which offer good detection limits despite suffering from matrix interference due to the high volatility of mercury which restricts the ashing temperature At the same time while mercury is one of the worst elements for detection

by flame-AAS (due to its tendency to form stable molecules in the flame), some researchers continue to look for new ways to improve this method.

Preconcentration of mercury can be easily done using traps based on the amalgamation of Hg with noble metals such as silver, platinum, and especially gold.[12] Mercury vapor is caught in these traps and later released via heating for detection. This allows not only preconcentration but also the ventilation of interfering substances from the gas stream before measurement.

Speciation of different mercury compounds (Hg^0, Hg_2^{2+}, Hg^{2+}, organomercurials etc.) can also be carried out either on line with species detection or off-line with total mercury determination. The speciation of mercury compounds is important due to the varying levels of toxicity associated with the different forms which Hg can take. Of particular interest are methylmercury compounds, not only because they are highly toxic but also because mercury can be methylated in the environment (especially marine and freshwater sediments) and accumulated in the tissue of fish, continuing up the food chain.[13,14] When mercury in any form and from any source enters the environment, it can be converted into its toxic methyl derivative. The chemical pathways for the methylation of mercury in the environment have been reviewed.[15] Chromatographic techniques are most commonly used for speciation, including GC, HPLC, and ion chromatography.

Cold Vapor Atomic Absorption Spectrometry

No Preconcentration

The cold vapor (CV) technique was originally developed as an introductum method for atomic absorption spectrometry (AAS), although it was later used for other techniques (most notably AFS). For this reason, a review of the literature of the development of AAS of mercury is also the story of the development of the cold vapor technique.

The first instrument based on the absorption of UV (253 7 nm) light by mercury vapor was proposed by Woodson in 1938 to detect Hg in flue gas from a mercury boiler [7] It was reported to be small and portable, with a useful range of 1 ppm - 1 ppb The cold vapor atomic absorption procedure as it is known today, is typically attributed to Hatch and Ott [16] Reduction of dissolved solid samples occurred by tin (II) sulfate after which aeration occurred carrying the vapor to a 25 mm × 15 cm glass tube with quartz windows A detection limit of 1 ppb in solution was reported.

Five years later Gilbert and Hume[17] reported an improvement on the technique, which involved a more efficient aeration technique, reducing analysis time and yielding an LOD (defined as 2σ of the blank) of 0 4 ppb or 4 ng absolute In addition to using tin (II) chloride as a reducing agent, it reported and referenced the use of oxidizing agents permanganate and persulfate to maintain Hg in the divalent, nonvolatile state and UV irradiation and hot acid to destroy organic matrices and organomercurial compounds

In 1996 Zhou *et al* [18] compared four different acid mixtures for high-pressure microwave digestion methods for determining total Hg in sediments After comparing HNO_3/H_2SO_4 $HNO_3/HClO_4$ HCl/HNO_3 and $HCl/HNO_3/HF$ aqua regia was chosen as it was time saving less dangerous, and suitable for other trace metal analyses Good recoveries (94 - 104%) were obtained from different soil and marine sediment matrices. The advantages of using sodium borohydride as the reducing agent for Hg in solution was discussed by Toffaletti and Savory[19] and Rooney.[20] Rooney reported a 10-fold increase in signal when using $NaBH_4$ rather than $SnCl_2$ giving a detection limit of 20 ng absolute However, he also noted that an $NaBH_4$ solution must be used within one hour of preparation Yamamoto *et al* [21] found that while both reducing agents yielded similar calibration curves and limits of detection, the precision using $NaBH_4$ was 2 5%, while for $SnCl_2$ it was 4 9% In 1988 Welz and Schubert Jacobs[22] also compared the two reducing agents. They claimed $NaBH_4$ performed as well as or better than $SnCl_2$ as a reducing agent for Hg in addition to reducing most of the organic compounds in solution Despite these results, most papers encountered in this review utilized the more robust $SnCl_2$, due to its longer shelf life and less violently reactive nature

In 1996 Brindle and Zheng[23] compared different designs of gas-liquid separators for sequential injection CV-AAS, including two Perkin-Elmer designs a spray chamber system, and a frit-based design Their comparison was based on efficient stripping of the analyte from solution and a small dead volume to ensure minimal dilution of the analyte with the carrier gas. They determined the Perkin-Elmer FIAS Chemifold gas-liquid separator to be the best, with the frit-based nebulizer a close second although it experienced memory effects for high concentrations of mercury

A method for measuring a stationary rather than a transient signal of mercury vapor was reported by Tong. [4] An ordinary 4-cm UV-cell was used as both reducing and detection cell as the mercury was reduced in solution and partitioned between the aqueous and gas phase in the stoppered cell In this way, the sensitivity of the method was reported to be improved due to the minimum of dead volume as opposed to a flow through system A detection of 0 02 ppb or 0 1 ng absolute was achieved

Methods for continuous flow monitoring of Hg were reported by Oda and Ingle[25] and Goto *et al* [26] The Oda and Ingle technique involved a continuous sample introduction reduction vessel into which sample and reductant solutions were continuously fed and Hg was reduced and volatilized An LOD of 0 03 ppb was reported, which was observed to improve to 0 003 ppb with discrete sampling Goto *et al* utilized a method of continuous flow digestion, reduction and extraction in small bore tubes at slow flow rates A detection limit of 0 1 ppb was obtained using a gas-liquid separator and 8 µL flow cell

Mineralization processes for biological materials were compared for CV-AAS by Colina de Vargas and Romero [27] Both a cold mineralization (acid digestion at -10° C for 1 week) method and high pressure bomb digestion (at 130° for 2 5 hours) were found to result in no Hg losses due to volatilization or adsorption. While the cold mineralization process took more time, it was recommended for processing large numbers of samples. The accuracy of the method was determined by comparison with a tuna certified reference material

Yamada *et al* [28] reported the use of a mixture of $SnCl_2$ and $NaBH_4$ at acidic solution to reduce the interference of I with the detection of Hg. Iodide has been found to interfere with the reduction of Hg in solution This report attributed the interference to

the formation of Hg complexes with I⁻. In this way, 85% of Hg in the presence of I was recovered. This was noted to be of interest when measuring Hg in wastewater or sewage samples.

Saraswati *et al*[28] combined flow injection analysis (FIA) with CV-AAS in order to miniaturize and automate the method. They noted the improvement in speed, precision, and sensitivity the addition of FIA can offer. After correcting the signal for matrix suppression by standard additions, an LOD of 0.08 ppb in a zinc ore matrix was obtained. Hanna and McIntosh[29] described the determination of total Hg in environmental samples with FI-CV-AAS after on-line microwave digestion. The method was fully automated with a limit of detection of 0.035 ppb or 0.18 ng absolute and an RSD of 1.1%. Because the entire analytical process occurred in a closed system, opportunities for contamination are greatly reduced.

Determination of total mercury in environmental and biological samples was carried out by Murphy *et al*[31] using an FI method with microwave digestion. The use of FIA in this case allowed for the rapid analysis of between 20 and 30 samples per hour, with an LOD of 0.2 ppb or 0.1 ng absolute and a RSD of less than 10%.

Preconcentration

Dumarey *et al*[32] compared the use of activated charcoal, silver-coated sand, and gold-coated sand as mercury collectors. It was noted that sheets or grains of Ag or Au show considerable memory effects and poor reproducibility. In their comparison, activated charcoal was found to be unsuitable as it had a high capacity for collecting interfering compounds and Hg desorption was incomplete at 600° C. When Ag-coated

sand was used description was fast and complete but organomercurials were poorly absorbed. In addition, on prolonged use of the Ag coating it was slowly converted to the sulfide resulting in a slight decrease in response. Au-coated sand was the only collector to retain the total content of volatile Hg compounds and was unaffected by sulfur compounds. In 1965, Dumarey *et al*.[33] made a similar comparison. This time they reported that activated charcoal and Ag-coated sand as absorbers suffered from poor quantitation and were dependent on sampling flow rate and duration, the nature of the mercury compounds and interfering substances. It was reported that the Au-coated sand amalgamation traps showed a quantitative collection for a sampling flow rate up to 5 L min^{-1} when heated to 600° C. Yoshida and Motojima[34] reported the use of Au-coated quartz wool as a mercury collector which was then heated to 650° C for rapid determination of Hg in air. They noted that the performance of the trap deteriorated after ten uses. Most of the papers encountered in this review used Au-coated sand as the collector.

Another determination of Hg in air was reported by Fitzgerald and Gill.[35] In this method, a two-stage Au amalgamation for atmospheric analysis of Hg was used. A field sampling technique was employed in which the major volatile Hg species in the near ground atmosphere were collected on Au coated beads, and atmospheric particulates were collected on glass fiber filters. The two-stage Au amalgamation technique was reported to separate interfering substances from the Hg vapor before the Hg was released to the detector. With this method, good precision and a good detection limit were achieved with an inexpensive single beam instrument. An LOD (2σ) of 0.06 ng absolute was reported with 4% RSD.

In 1974 Olafsson[36] reported the use of amalgamation on Au foil strips coupled to CV-AAS to detect Hg in seawater. After collection, the trap was heated to 300° C. Interferences included I⁻ and Br⁻. Fresmann and Schmidt[37] reported the use of an Au-coated silica wool plug in a 50 mm column as an amalgamation trap for determination of Hg in seawater. A Teflon sampling bottle was also used as the reaction vessel to reduce sample contamination. An LOD of 0.5 ppt or 50 pg absolute was reported with a 4% RSD. Welz *et al*[38] reported a method for picotrace (<1 ng/L) determination of mercury. After studying various amalgamation methods, they determined a gold/platinum gauze (90% Au, 10% Pt) to work the best due to its excellent sensitivity and reproducibility and because it could be easily cleaned in hot HNO_3. They also reported that $SnCl_2$ was superior to $NaBH_4$ as a reducing agent when using amalgamation, despite the higher, faster reducing power of $NaBH_4$ and its ability to decrease interferences such as I and Se. This was because the reduction reaction of $NaBH_4$ was a violent reaction, which could cause water droplets to be carried with the gas stream to the amalgamation trap, contaminating and deactivating it. At the same time, $NaBH_4$ was used for hydride generation of elements which were not normally volatile, allowing them to be carried with the gas stream and interfere with the detection of Hg. In addition, they recommended the use of PTFE tubing over silicone to avoid memory effects, He as the purge gas over Ar and N_2 due to its superior stripping efficiency, and $Mg(ClO_4)_2$ or H_2SO_4 over $CaCl_2$ as the desiccant to avoid capture of Hg. The method was reported to have good accuracy.

Temmerman *et al*[39] reported a method for determining Hg in drinking water after Au-coated sand amalgamation. An absolute LOD of 0.6 ppt or 0.6 ng absolute with

>10% RSD was reported. A method for measuring picomolar concentrations in seawater involving two-stage Au amalgamation was reported by Gill and Fitzgerald [40]. An LOD of 0.84 pM (0.042 pptr) or 0.084 ng absolute was determined. Welz *et al* [41] used an on line microwave digestion method to determine total Hg, including organics, in water and urine. It was noted that on-line sample pretreatment was of interest because of problems due to contamination, volatilization, and adsorption losses when the sample was transported. An LOD of 10 pptr or 0.1 ng absolute was reported for water samples using a flow injection method. Good agreement with certified values was obtained for urine samples. A similar study by Hanna *et al* [42] compared on- and off-line oxidation of organomercury compounds in water and urine for total mercury detection. An on-line LOD of 0.23 ppb or 0.12 ng absolute with 1.4% RSD was reported, with simplified sample pretreatment and an elevated operating temperature. An automated FI-CV-AAS method using Au gauze amalgamation was used by McIntosh.[43] A detection limit of 2 ppb or 17 ng absolute was reported. Stresko *et al.*[44] used a collection method utilizing the chelating ion exchanger Spheron Thiol for the preconcentration of mercury. This took advantage of the affinity of Hg for SH groups. An LOD of 0.05 ppb or 0.05 ng absolute of water was achieved with an RSD of 10%. Garcia *et al.*[45] compared different Hg chelate forming reagents (diethyldithiocarbamate, pyrrolidin-1-dithioformate and diphenylthiocarbazone [dithizone]) for the preconcentration of ultratrace amounts of inorganic Hg and CH_3Hg. It was observed that the carbamate type reagents performed superiorly to dithizone for on line concentration, and volumes of 100 mL could be preconcentrated with 100% efficiency for both inorganic mercury and methylmercury

Detection limits of 16 ppbr or 0 4 ng absolute of mercury were achieved, and the method was successfully applied to seawater samples

In 1976 Matsunaga and Takahashi[46] reported the detection of organic Hg in sediments and aquatic organisms by extraction of the organomercurials with benzene, back extraction, oxidation with potassium permanganate and persulfate, and preconcentration of Hg using Au granule amalgamation. With this technique, they were able to detect nanogram levels. Determination of Hg in environmental standard reference materials using pyrolysis to release Hg vapors, which were preconcentrated using a two-stage Au absorber system for CV-AAS, was reported by Dumarey *et al.*[47] This method was reported to be rapid and simple and free from the contamination of wet digestion. A detection limit of 5 ppb, or 0 1 ng absolute was reported. Vermeir *et al.*[48] reported a method of determining mercury in biological samples after high pressure HNO_3 digestion in a Teflon bomb Detection occurred after a two-step Au-coated sand amalgamation. An absolute LOD of 12 ppbr or 0 12 ng absolute was reported, along with results in excellent agreement with certified reference material values Horvat *et al*[49] described the use of Au amalgamation CV AAS for the determination of total Hg in coal fly ash Digestion was carried out with acid in sealed Pyrex tubes to prevent losses by volatilization. The results showed good agreement with the certified values and results obtained by neutron activation analysis Brandvold *et al*[50] reported a novel combustion method of determining Hg in solid samples. Gaseous mercury was evolved when a solid sample is heated above 500° C in the presence of oxygen. The evolved Hg was collected on Ag wool, and 95% recovery was observed for various sediment and ash standards The LOD (2σ) was observed to be 2 3 ng absolute

Ombaba[51] reported the use of an amalgamation tube (MAT) containing Au sites to preconcentrate Hg from environmental and biological standard samples followed by CV AAS. The samples were microwave digested under high-pressure and reduced with $SnCl_2$. Good agreement was found with several certified reference material values at sub-ppm levels.

Flame Atomic Absorption Spectrometry

Ellis and Roberts[52] reported the use of a Au-coated dual 'bent' tube atom trap in order to improve the normally poor sensitivity encountered with flame AAS. Mercury was collected in the trap thereby reducing its volatility. It was determined that low fuel flow, percentage obscuration and high tube height were important for maximum sensitivity, and a precision of 2.9% was achieved. A comparison with CV-AAS found the results to be in close agreement, although not as sensitive.

Electrothermal Atomization Atomic Absorption Spectrometry

Trace levels of Hg were determined without preconcentration by Keller *et al*[53] using electrothermal atomization (ETA)-AAS with uncoated graphite furnace cuvettes. A detection limit of 0.6 ppb or 0.03 ng absolute was reported. The method was applied to samples of drinking water, and was found to report results in good agreement with USEPA reference standard values.

Hladky *et al*[54] determined mercury concentrated in mineral acids (HCl, H_2SO_4 and H_3PO_4) using an Au-coated graphite furnace cuvette, from which the absorbance was

read after the release of the Hg from the amalgam. The amalgam prevented analyte loss and removed nonspecific absorption and water vapor from the matrix, detecting concentrations from 100 to 5 ppb with a 15% RSD. Lee *et al*[55] reported the determination of Hg in environmental samples by a combination CV/Au-coated graphite furnace technique. A detection limit of 0.1 pptr or 5 pg absolute was determined with an RSD of 2.7%. Analytical results were obtained for natural waters, marine biota, and sediments. Siemer and Haganian[56] reported the determination of Hg in water using Au coated graphite furnace atomizer tubes which were then placed into either a carbon rod atomizer or a Woodriff furnace. A detection limit of 14 ppb was reported.

Baxter and Frech[57] reported the use of a Pt-lined graphite furnace for *in situ* preconcentration of Hg, which was produced after the reduction of water samples. An LOD (2σ) of 2 pptr or 0.1 ng absolute was determined, and synthetic seawater samples were analyzed.

Speciation Coupled with Atomic Absorption Spectrometry

Rapsomanikis and Craig[58] reported a method of gas chromatography (GC) separation of organomercury compounds with quartz furnace AAS detection. Because CH_3Hg^+ is co-eluted with $(CH_3)_2Hg$ or Hg^0 causing difficulties in speciation, they performed an ethylation of CH_3Hg^+ in aqueous ethanolic solutions with $NaB(C_2H_5)_4$ and detected the resultant compounds. An oven temperature of 100° C was used, and an absolute detection limit of 123 ppb or 167 pg absolute for CH_3HgCl was observed. Fischer *et al*[59] then applied this derivation method to the determination of CH_3Hg in fish

after dissolution in an alkaline methanolic solution. The detection limit was observed to be 4 ppb or 4 pg of CH_3Hg^+ as $C_2H_5HgCH_3$ and 75 ppb or 75 pg absolute of Hg^{2+} as $(C_2H_5)_2Hg$.

A method described by Emteborg *et al* [60] used a preconcentration step with a dithiocarbamate resin before GC separation. In addition, simultaneous use of two wavelengths (184.9 nm and 253.7 nm) for absorption and a 2.4 cm cuvette improved the dynamic range and sensitivity, which resulted in LODs of 0.03 ppm or 0.03 ng absolute for CH_3Hg^+ and 0.4 ppm or 0.4 ng absolute for Hg^{2+}.

Ahmed *et al.*[61] used an anion exchange column to separate CH_3Hg^+ from Hg^{2+} in rain samples. The CH_3Hg^+ was then decomposed by UV irradiation. Different acids at different concentrations were compared for decomposition and percent recoveries. Saraanni *et al* [62] reported the use of cation exchange ion chromatography to separate Hg compounds after *in situ* cysteine complexation ($Hg(Cys)_2$, CH_3HgCys, and C_2H_5HgCys). Detection limits of 20 ppm or 2 ng absolute for Hg^{2+}, 100 ppm or 10 ng absolute for CH_3Hg^+ and 40 ppm or 4 ng absolute for $C_2H_5Hg^+$ were reported, and the method was applied to synthetic mixtures and natural samples.

Liquid chromatography (LC) was coupled with CV-AAS with a continuous flow reducing vessel by Fujita and Takabatake.[63] Tin(II) chloride was used to reduce Hg alkane thiolates; reduction of inorganic, methyl, and ethyl mercuric compounds was carried out with $NaBH_4$. The authors reported high sensitivity and selectivity. Azcpun *et al* [64] reported a method of HPLC-CV-AAS for the speciation of inorganic Hg^{2+} and CH_3Hg^+ using vesicles of didodecyldimethylammonium bromide (DDAB), rather than an organic solvent, as the mobile phase. The use of DDAB vesicles was reported to improve

CV generation of Hg. Before separation, off-line preconcentration of the aqueous samples was carried out using C$_{18}$ Sep-pack cartridges modified with 2-mercaptoethanol solutions. LODs of 0.1–0.2 ppb of Hg were achieved, and the method was applied to spiked seawater and human urine.

Baker's yeast cells (*saccharomyces cerevisiae*) were used to separate CH_3Hg^+ and Hg^{2+} by Morlod *et al*.[65] with good recoveries. The percentage of CH_3Hg^+ fraction bound to the yeast cells did not depend on the experimental conditions tested, while the retention of Hg^{2+} depended on analyte concentration, biomass, and incubation time.

Flame Atomic Fluorescence Spectrometry

Atomic fluorescence spectrometry (AFS) was first used to determine Hg by Winefordner and Staab in 1964.[66] LODs of 5 ppm in a H_2/O_2 flame and 1 ppm in an C_2H_2/O_2 flame were achieved. These LODs were compared to an LOD of 25 ppm of which F-AAS was capable at the time.

Cold Vapor Atomic Fluorescence Spectrometry

No Preconcentration

Although CV-AAS has been the most common method for the detection of mercury for decades, AFS is increasingly being used today. AFS is currently the US Environmental Protection Agency preferred method for determining Hg in water (Method 1631). It has a larger linear dynamic range and an inherently high sensitivity capable of

measuring lower detection limits. In addition, it suffers from fewer interferences than AAS.

Hutton and Preston[67] reported the use of a non dispersive AFS instrument using CV generation in order to improve the detection limit for Hg. It was noted that the instrument compared favorably with other CV systems, but without complex instrumentation. An LOD of 0.04 ppb or 0.04 ng absolute was reported with a precision of 2-3%. A flow injection method was employed by Morris *et al*[68]. Mercury fluorescence was detected at both 184.9 and 253.7 nm, and an LOD of 0.12 ppb (8 pg absolute) was determined.

Swift and Campbell[69] reported the determination of Hg in environmental samples after microwave digestion. A detection limit of 1.3 ppm was achieved, and the method was applied to water and soil samples. Lamble and Hill[75] described the use of batch and on-line microwave digestion of slurried environmental samples for the determination of total Hg. An LOD of 13 ppm was reported with 1.5% RSD, as well as good agreement with certified reference material values of dogfish muscle and marine sediment.

Stockwell and Corns[71] discussed the detection of Hg using a Merlin fluorescence detector with which they achieved an LOD of 0.37 ppm in 50 mL. Janjic and Kiurski[72] used CV AFS to detect Hg in river water samples and achieved an LOD of 0.001 ppm with a RSD of 3%.

Corns *et al*[73] described a method of determining Hg in urine samples using an automated continuous flow CV-AFS system with bromine oxidation. An LOD of 1 ppm or 50 pg absolute was achieved. Bloxham *et al*[74] reported the use of bromination digestion for determining Hg in filtered seawater. In a flow injection method, on-line

oxidation of organomercurials was used. Detection limits of 25 ppth or 0.5 pg for HgCl and 23 ppth or 0.5 pg for CH_3HgCl were reported as well as good agreement with certified values for lobster hepatopancreas.

Preconcentration

In 1972, Muscat *et al.*[75] described a CV-AFS method for determining Hg using amalgamation with an Ag wire for preconcentration. An absolute LOD (2σ) of 0.6 pg was observed with an RSD between 10-20%. Mercury concentrations in certified materials and natural sediments were determined. Ferrara *et al.*[76] reported the use of Au wool for preconcentration of Hg in seawater. A Hg radiofrequency electrodeless discharge lamp was used as an excitation source. A detection limit of 0.01 ng was achieved.

A method involving flow injection of Hg vapor to a Au wire absorber for preconcentration was described by Chan and Sadana.[77] The method was used to determine Hg in water samples, had a detection limit of 2 ppth or 54 pg absolute and 3% RSD was obtained. Cossa *et al.*[78] described a method of determining Hg in natural waters using preconcentration on Au-Pt gauze. The automated method analyzed eight samples per hour with a detection limit of 0.1 ppth or 4.5 pg absolute with 5% RSD. These same authors later reported a method of automated Hg determination in waters with the same LOD and precision.[79]

Poissant *et al.*[80] reported the first telemetry and remote sensing design for an atmospheric Hg analyzer based on CV-AFS with Au amalgamation preconcentration.

This fully automated portable system permitted easy on-site monitoring, real time data acquisition and was usable in hazardous environments or in remote areas

Electrothermal Atomization Laser Enhanced Atomic Fluorescence Spectrometry

One of the advantages of AFS over AAS is that using more intense light sources can result in more sensitive measurements Resto *et al.*[81] reported the use of electrothermal atomization two-step laser enhanced AFS (ETA-LEAFS) of Hg vapor in a graphite furnace An excimer laser was used to pump two tunable dye lasers, set at 253 7 nm and 435 8 nm. A detection limit of 9 pptr or 90 fg absolute was achieved by measuring the atomic fluorescence at the 546 1 nm line In addition, a linear dynamic range of seven orders of magnitude was reported Pagano *et al.*[80] used this method to determine total mercury in microwave digested soils and achieved a detection limit of 1 4 pptr or 14 fg absolute which was the lowest reported absolute LOD for total Hg

Inductively Coupled Plasma Atomic Fluorescence Spectrometry

Lancione and Drew[83] used a commercial instrument with inductively coupled plasma atomic fluorescence spectrometry (ICP-AFS) and some modifications to determine Hg Simultaneous element detection was possible with this instrument, and an LOD of 200 pptr was achieved In the single element detection mode, the LOD was 40 pptr

Speciation Coupled with Atomic Fluorescence Spectrometry

Gas chromatography (GC) was coupled to CV AFS by Bloom and Fitzgerald[84] for Hg determination after preconcentration from air on a Carbotrap column. The column temperature was ramped to 180° C over 20 minutes. The detection limits achieved were 0.3 pg for Hg and $(CH_3)_2Hg$. 0.4 pg for $(C_2H_5)_2Hg$, and 2.0 pg for CH_3HgCl. Sanzolone and Blattman[85] described a semiautomated analytical system for total Hg using GC AFS with Au-coated sand preconcentration. LODs of 0.07 pptr (1.4 pg absolute) for aqueous and 1 ppb for tissue samples were reported. In addition, organic mercury was derivatized with $NaB(C_2H_5)_4$ before separation for detection limits of 0.05 pptr of CH_3Hg^+ for aqueous samples and 1.4 ppb for tissue samples. Gas chromatography was employed by Jonas *et al*[86] for total and organic Hg determinations in water, soil, and tissue samples. Water samples were brominated and preconcentrated onto sulfhydryl cotton fibers and organic mercury was extracted into CH_2Cl_2 before being separated. Detection limits were 0.3 pptr or 0.6 ng absolute for inorganic Hg, 0.3 pptr or 0.6 ng for total Hg, and 0.02 pptr or 0.04 ng absolute for organic Hg, while in soil and tissue samples, the LOD for organic Hg was 0.2 pg absolute.

Jian and McLeod[87] carried out speciation on a column of sulfhydryl cotton for rapid sequential determination of Hg^{2+} and CH_3Hg^+ in natural water samples by FI-CV-AFS. The LOD was 6 pptr or 3 ng absolute.

Microwave Induced Plasma Atomic Emission Spectrometry

The advantages of microwave induced plasma atomic emission spectrometry (MIP-AES) include its high detection power, inherent multielement capability large linear dynamic range, and high selectivity A problems with interferences is one disadvantage.

In 1994 Camuña-Aguilar *et al* [88] compared three Ar and He MIPs for AES used specifically for excitation of Hg and its determination after on-line continuous CV generation. The He plasmas were found, by comparison of the analytical figures of merit, to be superior to the Ar plasmas for excitation of Hg The best LOD for Hg, 10 pptr was achieved with the He surfatron with a 1 mm i d. fused silica tube as the plasma torch In addition, a linear dynamic range of over three orders of magnitude was reported and a RSD of 4% but the plasma was influenced by the entrance of molecular gases and water vapor The application of these plasmas to seawater was studied

An atmospheric pressure He MIP was used by Tanabe *et al.*[89] to determine Hg from solution An LOD of 4 pptr or 8 pg absolute with 2% RSD was reported with a linear dynamic range of 2×10^5 Interferences were negligible except for Pt^{2+} and Pd^{2+} Good agreement was reported with certified reference material values for bovine liver Nojiri *et al*[90] reported the determination of Hg in lake water with an atmospheric pressure He MIP using a Au-coated pumice amalgamation trap for preconcentration An LOD of 0 01 pptr in 50 mL or 0 5 pg absolute was reported. Natarajan[91] reported the use of a low power Ar MIP with amalgamation on Ag wool of Hg in solution Determination of 50 pptr or 0 5 ng absolute is reported, and a detection limit of 0 1 ng is reported

An atmospheric He MIP with an automated gas handling system for GC-AES detection was reported by Quimby and Sullivan [93]. The system was optimized for microwave cavity, discharge tube, and gas flow system. Sensitivities for several elements were reported, the sensitivity for Hg was found to be 0.1 pg/s.

Tao and Miyazaki[93] reported the simultaneous determination of Hg with other elements subjected to hydride generation (HG) using a He MIP with a hydrogen separation membrane. The latter prevented byproducts of HG (H_2, CO_2, HCl, H_2O) from reaching the plasma which could be extinguished. A detection limit of 0.50 ppb for Hg was reported. Siemens *et al.*[94] reported the use of atmospheric pressure He and Ar MIPs for the continuous monitoring of Hg in flue gases. Both TM_{010} cavity (Beenakker resonator) and surfatron-type plasmas were tested. The detection limit of Hg in nitrogen was 8 μg m^{-3} for the TM_{010} MIP and 10 μg m^{-3} for the surfatron. The addition of main flue gas components such as H_2O vapor, O_2, and CO_2 were found to suppress Hg lines considerably.

Inductively Coupled Plasma Atomic Emission Spectrometry

Nakahara and Wasa[95] reported a method using direct nebulization of the reductant solution for the determination of mercury with inductively coupled plasma atomic emission spectrometry (ICP-AES) in order to increase transport efficiency. Reducing agents $SnCl_2$, Na_2SO_3, NH_2OH, and $NaB(C_2H_5)_4$ were compared as reducing agents and $SnCl_2$ was chosen as it gave the largest enhancing effect. An LOD of 1.3 ppb was reported with an RSD of 2.8%.

One problem associated with ICP AES is its difficulty in determining trace elements in biological samples In order to improve on this, Canada Rudner *et al* [96] reported a method of FI ICP-AES with on-line preconcentration based on complexation of Hg with 1,5-bis(di-2-pyridyl)methylene thiocarbonohydrazide (DPTH) and its subsequent extraction into isobutyl methyl ketone (IBMK) Reduction and extraction from the organic phase occurred and Hg vapor was generated, followed by detection. An LOD of 2 ppb or 20 ng absolute was reported with 3 3% RSD and few interference problems were encountered These authors later reported a similar method[97] with which they obtained an LOD of 4 ppb or 40 ng absolute with 1% RSD Human hair, pig kidney, and dogfish muscle samples were analyzed with good agreement with certified values Andersen *et al* [98] reported a method for determining Hg in sediment and tissue samples using acid (HNO_3) digestion and heated permanganate oxidation, followed by $NaBH_4$ reduction and CV introduction into the plasma The emission wavelength used was 194 2 nm and a detection limit of 2 ppb or 20 ng absolute was reported Excellent correlation with certified reference material values for environmental samples was achieved.

Jamousi *et al* [99] reported the use of ICP AES to determine heavy metals in honey Determination was carried out after high pressure microwave digestion A detection limit of 0 05 ppb or 5 ng absolute for Hg was reported, and the method was applied to honey samples from farms in north Tunisia It was observed that concentrations of heavy metals lower than the safety levels established by the World Health Organization could be detected

DC Discharge Plasma Atomic Emission Spectrometry

A method for continuous flow CV determination of Hg by AES using reverse FI was reported by de Andrade and Bueno[100] using dc discharge He plasma atomic emission spectrometry (DCP-AES). The gas stream from the gas-liquid separator was used as the plasma medium. Preconcentration on Au foil was carried out, and a detection limit of 50 pptr or 50 pg absolute was achieved with an RSD of 1 6% Good agreement was reported with certified reference material values for human hair

Ring Discharge Plasma Atomic Emission Spectrometry

Wrembel[101] reported the use of ring discharge plasma AES with amalgamation preconcentration for determining Hg The detection limit in pure water was found to be < 0.5 pptr The method was applied to synthetic and natural seawater samples.

Speciation Coupled with Atomic Emission Spectrometry

Gas chromatography (GC) was coupled with MIP-AES by Decadt *et al* [102] for semiautomated headspace analysis of biological samples. This method was used to assess gas-liquid coefficients of CH_3Hg^+ halides dissolved in water or benzene The highest vapor concentration was found to be for CH_3HgI. The method was applied to a series of biological samples with a detection limit of 1 5 ppb The use of a headspace sampler lessened column degradation as opposed to direct on-column injection Lansens *et al* [103] used preconcentration of CH_3Hg^+ on a column of dithiocarbamate resin before converting it to the iodide and performing detection by headspace GC-MIP-AES

Emteborg *et al.*[104] reported the preconcentration of CH_3Hg^+ and Hg^{2+} from humic-rich water on a dithiocarbamate resin. The Hg species were extracted and butylated before GC injection and detection by MIP-AES. Good recoveries were reported with LODs of 0.04 ppb or 40 ng absolute for CH_3Hg^+ and 0.28 ppb or 280 ng absolute for Hg^{2+}. A purge-and-trap method of injection, which involved ethylation of the ionic species before cryogenic trapping and subsequent MIP AES was reported by Cenimans and Adams.[105] LODs of 0.6 pptr or 6 pg absolute for CH_3Hg^+ and 2 pptr or 20 pg absolute for Hg^{2+} were found, and river and soil run-off samples were analyzed.

An alternating current He plasma detector was developed for GC detection by Costanzo and Barry.[106] A sensitivity of 20 pg/s for C_2H_5HgCl and 3.5 pg/s for CH_3HgCl with a linear dynamic range of 3 orders of magnitude was reported.

High performance liquid chromatography (HPLC) was coupled with ICP-AES with post-column CV generation by Kruli *et al.*[107] for Hg speciation. The ICP used had an all glass chamber, which decreased the memory effects typically found with a polypropylene spray chamber. Detection limits (2σ) were 37 ppb or 16 μg absolute for CH_3HgCl, 62 ppb or 31 μg absolute for CH_3CH_2HgCl, 35 ppb or 18 μg absolute for $HgCl_2$, and 62 ppb or 31 μg absolute for $(CH_3)_2Hg$. Costa Fernandez *et al.*[108] coupled HPLC with MIP AES with CV generation. The vesicle-forming surfactant DDAB was employed as the HPLC mobile phase increasing emission signals by 75%. Detection limits of 0.15 ppb for inorganic Hg and 0.35 ppb for CH_3Hg^+ were achieved, and the method was applied to natural water and human urine samples.

Photoacoustic Spectrometry

Patterson[109] reported the use of a differential photoacoustic mercury detector to determine Hg by photoacoustic spectrometry (PAS). Gold foil within the two cells collected the Hg, and the difference between the two concentrations was measured as the differential between the photoacoustic signals, detected by microphones. An LOD of <0.02 ng Hg absolute was reported.

Chen *et al*.[110] reported the use of PAS to detect Hg^{2+} as Hg(II) dithizonate in the solid state. Mercury(II) was extracted to the organic phase as $Hg(HDz)_2$ which, under irradiation of strong visible light, underwent a reversible photochromic reaction which changed its absorption wavelength from 405 nm to 620 nm. This corresponded to an excited state of $Hg(HDz)_2$. This excited state was detected by PAS using a He-Ne laser. In this way, a detection limit of 3 ppm was achieved, with the absence of interferences because only $Hg(HDz)_2$ exhibited photochromism in the solid state. Chen and Lai[111] later reported the same measurement in organic solvents. They found a 1:1 v/v mixture of benzene and CCl_4 to be the optimum, with an LOD of 0.8 ppb.

Metastable Energy Transfer for Atomic Luminescence

Dodge and Allen[112] reported the use of metastable energy transfer for atomic luminescence (METAL) to detect trace amounts of Hg. At pressures of ~1 Torr, an electrical or microwave discharge in flowing nitrogen produced a metastable-state molecule which interacted with Hg in a reaction cell to produce a chemiluminescent reaction. Metastable state N_2 molecule has been shown to excite the 253.7 nm Hg

emission. This type of detection was reported to give a detection limit of 10^7 atoms cm^{-3} (3 ppq), which is the lowest reported concentration LOD. The method also had a linear dynamic range of 8 orders of magnitude.

Magnetically-Induced Optical Rotation

Magnetically-induced optical rotation (MIOR) was reported by Stephens[113] for determining Hg in vapor. Its advantages included automatic correction of continuum background absorption and of source drift. A detection limit of 10 pg absolute was achieved, and the method was noted to have good selectivity and sensitivity.

X-Ray Fluorescence Spectrometry

D'Silva and Fassel[114] reported a method of X-ray fluorescence spectrometry (XRFS) of Hg vapors in Ar. Good reproducibility and ppb levels of determination were achieved. Bilal *et al* [115] reported an energy dispersive XRFS method for monitoring Hg contamination. Samples of plant effluents from a lead battery plant were made into slurries and dried for analysis. The method was noted to be capable of yielding concentration profiles. A method of total reflection XRFS was reported by Holyńska *et al* [116] for analyzing potable water after preconcentration with a mixture of carbamates. A detection limit of 60 ppbr or 1.5 pg absolute was reported.

^{199}Hg Nuclear Magnetic Resonance Spectrometry

Methylmercury complexes were indirectly determined using ^{199}Hg nuclear magnetic resonance spectrometry (NMR) by Robert and Rabenstein[117]. The heteronuclear multiple quantum coherence (HMQC) method that was applied provided a significant sensitivity enhancement for the spectra of $CH_3Hg(II)$. The method was applied to the study of the solution chemistry of $CH_3Hg(II)$-thiol ligand complexes.

Laser Induced Breakdown Spectrometry

Lazzari *et al*[118] reported the use of time-resolved laser-induced breakdown spectrometry (LIBS) for the detection of Hg in air. A limit of detection of 5 ppb was reported, as well as good accuracy. It is recommended for *in situ* continuous monitoring of industrial processes in factories or plants.

Furnace Atomic Non-Thermal Excitation Spectrometry

Furnace atomic non-thermal excitation spectrometry (FANES) was used for determining Hg following reduction and *in situ* preconcentration in a Pt-gauze lined graphite tube by Baxter *et al*[116]. An absolute detection limit of 2 ppbr or 20 pg absolute was reported. Three standard reference materials - citrus leaves, pine needles, and river sediment - were analyzed after microwave digestion and accurate results were obtained for sub-ppb levels.

Inductively Coupled Plasma Mass Spectrometry

No Preconcentration

Inductively coupled plasma ionization coupled with mass spectrometry (ICP MS) has become a popular method for trace metal analysis since the 1980 s due to its superior selectivity and detection limits One disadvantage of detection of Hg is its high ionization potential (10 44 eV) and consequently poor degree of ionization in the ICP The method also suffers from matrix and memory effects

Haraldsson *et al.*[120] used ICP-MS for determining Hg in natural waters after reduction to its elemental form Sodium borohydride was used as the reductant rather than $SnCl_2$ to avoid contamination of the system with Sn. Determinations both with and without isotope dilution were carried out, the LOD for both was 0.08 ppbr or 8 pg absolute with an RSD of 2 7%. Natural waters and reference sediment samples were analyzed. Direct injection nebulization (DIN) was used to determine mercury in drinking water by Powell *et al* [121] DIN was compared to a conventional pneumatic nebulizer (PN) and was found to have a comparable detection limit (40 ppbr for PN 30 ppbr for DIN) with a drastic reduction in memory effects

Hydride generation (HG)-ICP-MS was reported by Brown *et al* [122] for determining Hg in biota. HG was compared to PN and was found to obviate memory effects to a great extent An LOD of 100 pptr in urine is reported.

Preconcentration

Flow injection with preconcentration on Au Pt gauze to detect Hg in water samples was reported by Debrah *et al* [123] An LOD of 0 2 pptr or 5 pg absolute with 1% RSD is reported The method was used to determine Hg in seawater and freshwater reference materials with good accuracy

Smith[124] reported the use of isotope dilution ICP MS for the determination of Hg in water and sediments. Preconcentration on Au foil was used Samples were submitted to 1Hr acid digestion and spiked with ^{201}Hg. An LOD of 0.2 pptr or 40 pg absolute was reported, and the method was used to analyze river water standards

Speciation Coupled with Inductively Coupled Plasma Mass Spectrometry

GC-ICP MS was used to determine that CH_3Hg^+ was the only significant organomercury compound in two marine biological standard reference materials by Beauchemin *et al* [125] Analysis of the samples was done by extracting the CH_3HgCl from the material with toluene and back extracting into an aqueous medium of cysteine acetate Isotope dilution and FIA were used in the sample introduction. Detection limits of 4 0 ppb or 1 ng absolute for ^{201}Hg and 2 2 ppb or 0.55 ng absolute of ^{202}Hg with FIA were determined with 7% RSD Excellent agreement with certified values for dogfish muscle and lobster hepatopancreas was achieved. Hintelmann *et al* [126] used GC-ICP MS to measure methylation rates of mercury in sediments with enriched stable Hg isotopes combined with CH_3Hg^+ determination. Methylmercury was converted to $CH_3HgC_2H_5$ using $NaB(C_2H_5)_4$ and preconcentrated on a Tenax adsorber A detection limit of 0 02

ppb or 1 pg absolute with 4% RSD was reported. Mercury methylation was investigated by spiking sediments with stable enriched Hg isotopes at *in situ* concentrations so as not to disturb the system. More than 3% of the added Hg was found to be methylated after an incubation period of 21 days

Speciation by LC ICP-MS was carried out by Bushee with post-column cold vapor generation [127] The method was found to be linear over 3-4 orders of magnitude with detection limits (2σ) of 0 6 ppb for $CH_3HgOOCH_3$, 1.2 ppb for $HgCl_2$, and 1 2 ppb for CH_3CH_2HgCl. Good agreement was obtained for a tuna certified reference material and for the detection of thimerosal in contact lens solution. Shum *et al.*[128] used a microbore column reversed-phase LC-ICP MS with DIN to speciate Hg and Pb compounds A detection limit of 7 pg absolute was achieved for Hg. It was reported that the urine samples analyzed did not contain sufficient organomercurials to be detected, however, good separations were obtained when these compounds were spiked into the sample

Reversed-phase LC-ICP-MS with ultrasonic nebulization was reported by Huang and Jiang [129] Detection limits were reported as 0 7 ppb or 0 14 ng absolute for CH_3HgCl, 0 4 ppb or 0 08 ng absolute for $HgCl_2$, and 0 8 ppb or 0 16 ng absolute for C_2H_5HgCl, and were compared with other LC coupled methods. Samples of contact lens solution, waste water, and fish were all analyzed, and the results were found to be in good agreement with certified values Mercury species in seawater were determined by LC-ICP MS by Bloxham *et al.* using a C_{18} column [130] Detection limits in seawater of 0.25 ppb or 25 ng absolute CH_3HgCl and $HgCl_2$ and 0 75 ppb 0r 0 75 ng absolute C_2H_5HgCl were achieved.

Using off line preconcentration on a dithiocarbamate resin gave detection limits (2σ) of 16 pptr or 16 ng absolute for CH_3HgCl and 17 pptr or 17 ng absolute for $HgCl_2$

Spectrophotometry

The determination of Hg^{2+} and $C_6H_5Hg^+$ using polyurethane foam (PUF) thin-layer spectrophotometry was reported by Abbas *et al* [131]. The PUF was loaded with dithizone to allow preconcentration of Hg^{2+} and $C_6H_5Hg^+$. The detection limit (2σ) for Hg^{2+} was 5 ppb or 0.05 ng absolute and for $C_6H_5Hg^+$ 10 ppb or 0.1 ng absolute. Ag was found to interfere. A method involving the spectrophotometric determination of Hg as its dithizone complex in the presence of a neutral surfactant was reported by Singh *et al* [132]. The surfactant, Triton X-100, allowed both the ligand and complex to be water soluble so the analysis could be carried out in aqueous media. An LOD of 1×10^{-6} M (200 ppb) or 20 ng absolute Hg^{2+} was reported and the method was successfully applied to the analysis of a Hg-based pesticide. Ramesh[133] reported a method based on the spectrophotometric detection of an abstraction of CN^- from hexacyanoferrate(II) by Hg^{2+} in the presence of 4-(2'-thiazolylazo)resacetophenone oxime. The method allowed the determination of Hg down to 10 ppb or 1 ng absolute, and was noted to be highly sensitive and accurate.

The determination of Hg based on its inhibitory effect on horseradish peroxidase which was immobilized on solid supports was reported by Shekhovtsova and Chemetskaya.[134] The inhibition of the enzyme increased in the presence of thiourea. Detection limits were reported as 0.1-10 pptr depending on the specific indicator reaction

The reaction was complete in 15 minutes A later report by Shekhovtsova *et al* [135] determined Hg in natural water by this method In the presence of Fe, which is normally found in natural water A detection limit of 10 ppb with 6% RSD was reported

Trace amounts of Hg in wastewater were determined with p-azobenzenediazoaminoazobenzene sulfonic acid by Jiang *et al* [136] The compound formed a red complex (528 nm) with Hg^{2+} in the presence of Triton X-100 and NH_3NH_4Cl Spectrophotometric determination of the complex gave a detection limit of 6×10^{-8} M (12 ppb) or 0.5 ng absolute The only interference was Cd, which could be masked with nitrilotriacetic acid

Fluorimetry

In 1973 Holzbecher and Ryan[137] reported the first observation of a Hg-complex induced fluorescence (at 440 nm) with an Hg-thiamine complex. In this way, Hg in solutions with low salt concentrations could be detected down to 10 ppb or 1 ng absolute with 3 2% RSD Interferences included Fe^{2+} and Fe^{3+} Fluorimetry was used by Narinesingh *et al* [138] in a screening method for trace Hg analysis using FI, the method was based on the inhibitory effect Hg has on the enzyme urease Urease catalyzes the conversion of urea to carbon dioxide, by fluorimetrically monitoring ammonia using o-phthaladehyde as the fluorophore the activity of the enzyme could be determined and Hg concentrations could be detected down to an LOD of 2 ppb This screening method could also be used to determine other heavy metals as well

Summary of Techniques

It is clear from the papers reviewed here that CV AAS remains the most popular method for the trace detection of mercury. At the same time, CV-AFS is becoming more visible due to its simpler instrumentation and ultralow detection limits as evidenced by its approval by the U S Environmental Protection Agency.

Detection limits for Hg using plasma AES and ICP-MS are limited by the high ionization potential of Hg, which cannot be efficiently reached in most plasmas. Exceptions are the He MIP and ring discharge plasma, which combined with AES offers LODs comparable to those using CV-AAS and CV-AFS. An advantage of these methods is their simultaneous multielement capabilities.

Additional advantages of spectrometric methods include their amenability to automation and coupling with chromatographic methods for speciation. The use of chromatography to separate and speciate different inorganic and organic forms of Hg is of importance due to the varying toxicity of the different forms, especially in environmental samples. Ultralow level detection of CH_3Hg^+ species is especially important due to its high toxicity.

Lowering detection limits without loss of analyte to contamination will continue to be the main difficulties to overcome in the detection of Hg as research continues in the direction of analyzing real samples, such as sediments or biological tissues. In addition the speciation of different Hg compounds will continue to be critical as it becomes more clear the toxicity levels of the various forms.

In 1991 it was reported that as sampling techniques improved over just a few years, the estimates of Hg concentrations in one lake dropped by a factor of 500 [139]. As external contamination of real samples decreases it becomes increasingly clear the minimal concentrations and amounts of Hg which can pose an environmental and health threat. Improvements in sample handling and preparation along with increasingly sensitive techniques will be needed to face these challenges in trace analysis of Hg.

Resonance Ionization Spectroscopy

Principles

Among the most sensitive methods for the detection of atoms are ionization spectrometric techniques [140,141]. These methods came of age in the 1970s with the introduction of the tunable dye laser. With this, the necessary resonant, selective interaction of light with matter at a high photon flux became readily accessible. Since then, techniques have been developed which involve this process including resonance ionization spectroscopy (RIS), laser enhanced ionization spectroscopy (LEIS), and resonance multiphoton ionization spectroscopy (RMPIS). Often, all of these methods fall under the general heading of resonance ionization spectroscopy.

The principles of resonance ionization, laser enhanced ionization, and resonance multiphoton ionization are presented in Figure 2-1. In the cases of RIS, atoms are promoted from the ground state to a defined, or bound, excited state of higher energy due to the absorption of a photon at the atom's resonant wavelength. The excited atom then

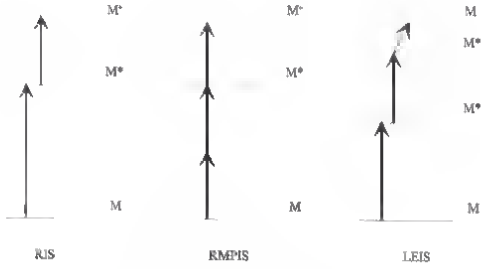

Figure 2-1 Processes of RIS RMPIS, and LEIS

usually absorbs another photon, of either the same or different wavelength. However, for atoms with low ionization energies, one photon may be sufficient to result in ionization. In this way, the atom is imparted enough energy to result in ionization by the loss of the high-lying electron.

In RMPIS, the absorption of two or more photons results in the excitation of the atom to a bound state. The absorption of one or more photons then results in the ionization of the atom from the excited state. Because of the absorption of multiple photons, rather than one of resonant energy, RMPI can be less selective than RIS.

In LEIS, one or more photons are absorbed to resonantly excite the atoms, as in RIS.[142] By increasing the number of resonance excitation levels or steps used, the selectivity of the method can be increased by orders of magnitude. However, ionization occurs not by the absorption of a photon. The atom gains the necessary energy to lose the electron by collisions with nearby atoms and/or molecules, such as in a flame or buffer gas. This process was originally referred to as the optogalvanic effect, as it depends on the application of an electric field to facilitate detection of the electrons. This ionization process is referred to as collisional ionization, rather than the photoionization process involved in RIS or RMPIS. In many cases, the ionization process is not limited to either photoionization or collisional ionization, but rather is a convolution of the two.

These techniques are inherently selective, due to stepwise resonance excitation, and sensitive, as 100% of the ions created may be detected by electrical means. Because of the typically lower collisional ionization efficiency from excited states as compared to the photoionization efficiency, RIS has typically been shown to be more sensitive. In fact, single atom detection was achieved by Hurst *et al.* in 1977.[142] In contrast, collisional

ionization has generally shown to be more selective than photoionization, and so LEIS is generally more selective than the photoionization methods.

Resonance Ionization Spectroscopy of Mercury

In 1981, Miziolek[144] reported the use of multiphoton ionization and emission analysis for the detection of Hg. This method involved the absorption of three 312.8 nm photons from a Nd YAG pumped dye laser to induce ionization of Hg atoms. Detection was carried out in two ways: (1) direct analysis of the ions and (2) detection of the 253.7 nm photons emitted by the recombined ions and electrons. Detection limits were 0.17 pptr using ion detection and 0.32 pptr for emission detection, which was limited by noise ion production from cell windows and nonselective multiphoton ionization of impurities.

The photoionization of Hg with isotope selection was reported in 1983 by Dyer *et al*[145]. The scheme of the three-step photoionization involved (1) excitation of the $6^1S_0 \rightarrow 6^3P_1$ transition with 254 nm radiation, (2) excitation of the $6^3P_1 \rightarrow 8^1S_0$ transition with 286 nm radiation, and (3) ionization from the 8^1S_0 state with 532 nm radiation. Laser radiation was produced by a Nd:YAG pump laser and two dye lasers. Isotopic information was obtained by monitoring fluorescence from the 6^3P_1 level and the ionization.

Normand *et al*[146] reported the use of three multiphoton ionization processes for mercury in 1983. The schemes involved (1) four-photon ionization through the $7p^1P_1$ level, (2) five photon ionization through the $6p^1P_1$ level, and (3) five-photon ionization through the $6d^1D_2$ or $^3D_2$ levels. Detection occurred by collection of ions or electrons.

In 1985 Bushaw[147] reported the use of double resonance multiphoton ionization for the determination of Hg. The process involved the excitation of the $6s^2\ ^1S_0 \rightarrow 6p\ ^3P_1$ transition with one photon of 253 73 nm radiation and ionization with two photons of 435 95 nm *via* the $7s\ ^3S_1$ state A detection limit of 220 fg was reported in ambient laboratory air

The pulsed optogalvanic effect with Hg was observed in a low-pressure mercury discharge by van de Weijer and Cremers in 1985 [148] This involved excitation of the $6p\ ^3P_1 \rightarrow 7s\ ^1S_0$ transition with 408 nm radiation from a nitrogen laser pumped pulsed dye laser It was reported that the ionization process was a two photon photoionization to an autoionizing level (a defined state which is above the ionization potential).

Kramer reported a pulsed laser optogalvanic effect observed in a high pressure Hg discharge in 1988 [149] An excimer pumped dye laser was used to excite the $6\ ^3P_{2,1,0} \rightarrow 7\ ^3S_1$ transitions with radiation of 546 436 and 405 nm respectively

In 1996 Matveev *et al.* developed a Hg resonance ionization photon detector (RID) [150] A three step process was used to excite the atom to a state very close to the ionization potential (1) $6\ ^1S_0 \rightarrow 6\ ^3P_1^0$ with 253 7 nm radiation, (2) $6\ ^3P_1^0 \rightarrow 7\ ^3S_1$ with 435 8 nm radiation, and (3) $7\ ^2S_1 \rightarrow 13\ ^1P_1^0$ with 489 0 nm With avalanche amplification of the signal, a detection limit of 0.5 photons was calculated.

CHAPTER 3
ANALYTICAL TIME RESOLVED RESONANCE IONIZATION SPECTROSCOPY

In resonance ionization spectroscopy (RIS),[142] the process of ion formation due to collisional ionization of analyte atoms can practically always be accompanied by their resonance photoionization and by non-selective ionization of molecules and/or atoms of buffer gas. Often, in order to improve the limit of detection one needs to acquire separate information about the contribution of the RIS signal bearing useful analytical information and the signal due to non-selective photoionization. This subject has been treated in several papers, together with the different concepts associated with the two definitions of ion yield and ionization efficiency.[151-5] Most work has been performed in flames operated at atmospheric pressure. Recently, it has been suggested[156] that when using flames as atomizers, this information can be obtained by observing a single time-resolved ionization waveform under conditions when the faster photoionization component and the slower collisional ionization component of the signal can be distinguished from one another. This idea can be extended to other atom reservoirs, such as a low pressure buffer gas. The deconvolution becomes possible when (1) the duration of the laser pulse is shorter than the average time in the collisional ionization process and (2) the distance between the collection electrode and the laser beam is less than the average distance traveled by the electron as a result of its drift velocity during the process of the collisional ionization, that is, the duration of the ionization signal from a single

electron should be less than the reciprocal of the rate of collisional ionization. This last condition is not always mandatory; in principle if one knows all of the experimental parameters including the mobility of electrons in a gaseous media, the configuration of the electric field between electrodes and certain parameters of the preamplifier and input circuit, information on photoionization and collisional ionization can be obtained by mathematical deconvolution of the computerized digital information from the signal waveform. However, the second requirement is necessary in this work, as it will allow signal that is due only to the analyte (collisional ionization) to be distinguished and extracted from the non-selective or background signal (photoionization and secondary ionization effects) without computerized deconvolution. It is essential to stress here that space charge effects must be absent. In fact, their presence would distort the shape of the ionization pulse and make their interpretation in terms of an ionization mechanism difficult.[156]

Time-resolved measurements of the current induced by the charges produced in a flame and in hollow cathode discharges have been theoretically modeled and experimentally observed.[142,157-61] However, the aim of these studies (with the exception of [149]) was to elucidate the process of charge detection, with the assumption that charge creation was instantaneous.

In this work, the temporal behavior of the ionization signal was studied in a quartz cell containing mercury vapor and a buffer gas at low pressure in order to elucidate the processes of ion formation. A three step excitation scheme for mercury[162] was utilized, in which the third step excited the analyte to a Rydberg level near the ionization continuum. Ionization signal waveforms were obtained by tuning the third laser step to

levels with different principal quantum number (n = 10-26) under different buffer gas pressures (0.05-600 Torr), with variable voltage and beam position between the electrodes. In this way, two clearly distinguishable components of the signal were observed, which could be attributed to collisional ionization and to photoionization.

Experimental

The experimental setup used in this work is shown in Figure 3-1 (M = mirror, BS = beam splitter). The inset shows a basic schematic of the ionization scheme. Three dye lasers (laser 1: Molectron, Portland, OR; lasers 2 and 3, Model Scanmate 1, Lambda Physik, Acton, MA) were pumped by an excimer laser (Model LPX-240i, Lambda Physik, Acton, MA) operated with XeCl (λ = 308 nm). The wavelengths of the three dye lasers are listed in Table 3-1. Laser dyes used include Coumarin 500 (Exciton, Dayton, OH), frequency doubled, for λ_{12}, Coumarin 120 (Lambda Physik) for λ_{23}, and Coumarin 153 and 47 (Lambda Physik) for the different λ_{34} wavelengths. The wavelengths of the first and second lasers remained constant, while the wavelength of the third laser was tuned to levels with different principal quantum number. Pulse energies were typically 150 mJ for the excimer, 20-100 µJ for λ_{12}, 200-300 µJ for λ_{23}, and 0.5-1 mJ for λ_{34}. Laser pulse durations were approximately 34 ns (FWHM), rather than the LPX-240i nominal duration of 14 ns.

The temporal behaviors of the three dye laser pulses is presented in Figure 3-2. Here, the output of dye lasers one, two, and three were observed with a fast photodiode (Model ET 2000, rise time <200 ps, Electro-Optics Technology, Fremont, CA) and

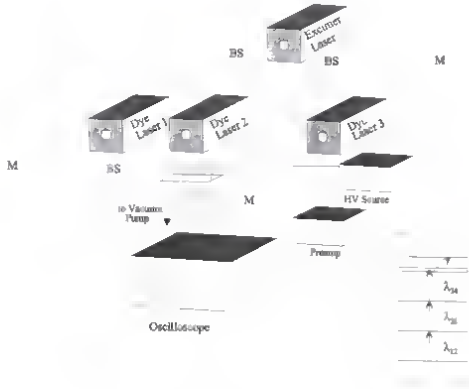

Figure 3-1 Experimental setup

Table 3-1 Excitation transitions for Hg for laser-connected levels 1, 2, 3, and 4 (Rydberg level), as tabulated by Moore[151] for n = 6,7,9-26

Excitation step	Level	Energy, cm^{-1}	Wavelength in air, nm
λ_{12}	$6p^3P_1^0$	39412.3	253.652
λ_{23}	$7s^3S_1$	62350.5	435.832
λ_{34}	$9p^3P_1^0$	79412.7	585.925
	$9p^3P_2^0$	79613.3	579.118
	$10p^3P_1^0$	80916.686	538.463
	$10p^3P_2^0$	81022.9	535.400
	$11p^3P_1^0$	81811.876	513.694
	$11p^3P_2^0$	81873.835	512.064
	$12p^3P_1^0$	82379.0	499.148
	$12p^3P_2^0$	82422.60	498.064
	$13p^3P_1^0$	82765.9	489.689
	$13p^3P_2^0$	82795.03	488.991
	$14p^3P_1^0$	83039.3	483.217
	$14p^3P_2^0$	83061.2	482.706
	$15p^3P_1^0$	83240.1	478.572
	$15p^3P_2^0$	83258.7	478.145
	$16p^3P_1^0$	83396.7	475.011
	$16p^3P_2^0$	83407.2	474.774
	$17p^3P_1^0$	83512.7	472.408
	$17p^3P_2^0$	83521.6	472.209
	$18p^3P_1^0$	83601.9	470.425
	$18p^3P_2^0$	83613.9	470.159
	$19p^3P_1^0$	83677.9	468.748
	$19p^3P_2^0$	83686.0	468.570
	$20p^3P_2^0$	83745.7	467.263
	$21p^3P_2^0$	83792.8	466.236
	$22p^3P_2^0$	83834.5	465.329
	$23p^3P_2^0$	83869.0	464.584
	$24p^3P_2^0$	83892.6	464.075
	$25p^3P_2^0$	83920.8	463.468
	$26p^3P_2^0$	83942.0	463.013

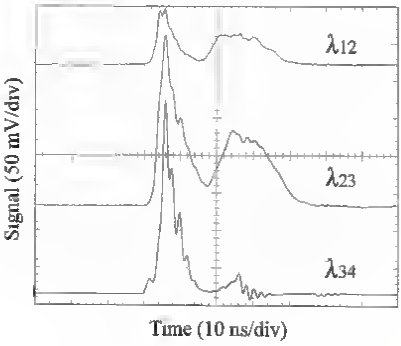

Figure 3-2 Temporal behavior of laser pulses

recorded with the fast digitizing oscilloscope (Model 602A, 500 MHz bandwidth Tektronix, Beaverton OR). Each pulse consisted of two maxima, the first more intense than the second, with a minimum in between them. After observing the pulse from the excimer itself, it was confirmed that this behavior was characteristic of the pump beam and not the dye output. At present, we have no explanation of such unusual behavior. However, rather than hindering our work, this behavior was very helpful in identifying the different sources of ionization. This is because in general, if one excluded those cases in which the electrons created have sufficient energy to modify the signal shape, any photoionization shape resembled the pulse which created it. In this work, the signal due only to photoionization was observed when only the first two laser connected steps were excited, λ_{12} and λ_{23}, so the photoionization resembles the shape of the λ_{23} because its power exceeds that of λ_{12} and is enough to saturate the third level. Therefore photoionization was very easy to identify and distinguish from other sources of ionization.

The beams were directed with mirrors and prisms into a quartz cell which contained a small amount of mercury and varying pressures of buffer gas (air or argon). At atmospheric pressure, the Hg number density in the cell was $\sim 4 \times 10^{13}$ cm^{-3}. The cell also housed two planar Ni electrodes and was connected to a vacuum pump. One electrode was connected to a high voltage source which applied varying potentials (0-1.5 kV) to the cell, while the other was connected to a low-noise high frequency preamplifier (Model 310, Sonoma Instruments, Santa Rose, CA). The amplified RIS waveform was displayed on a fast digitizing oscilloscope (Model 620A, Tektronix, Beaverton, OR). These waveforms were generated using different pressures, voltages, and beam positions

for different Rydberg levels with the goal of distinguishing between different ionization mechanisms.

Along with the experimental determinations, the ionization waveforms were theoretically simulated using DensMat,[164] a computer program which was used to model fully time-resolved simulations of two-step pulsed laser excitation of atoms in highly collisional media. The main purpose of this simulation was to estimate under what experimental parameters one should expect the duration of the pulse due to collisional ionization to exceed that due to photoionization. This program used the density matrix mathematical treatment of these processes and was very suitable for predicting the various level populations as a result of laser enhanced (collisional) ionization. The only incompatibility between this experiment and the model was because DensMat can only simulate a two-step excitation of three laser-connected levels, whereas our system consisted of four laser-connected levels. To adapt the three-step system to the dual laser model, the assumption was made that all of the atoms were excited to the first level of Hg during a short period of time (much shorter than the duration of the laser pulse), because the radiative lifetime of the $6p^3P_1^0$ state of Hg was much longer (118 ns) than the duration of the laser pulse and quenching was determined to be negligible, at the working pressures of the experiments, in both argon and air, we could consider this state having a steady state population during the period of laser irradiation. In this case, the λ_{23} and λ_{34} transitions corresponded to step one and step two in the DensMat simulation. In order to account for the loss in the ion population occurring at the electrodes, a non-laser connected level was added to the scheme as a trap in which the lost ions could accumulate (and not return to the ground state) just as occurred experimentally at the

electrodes The rate constant for this loss from the ion level to the trap was set as 1×10^{11} s^{-1} as it occurred at a higher rate than the collisional ionization from the third level to the ionization continuum The rate constants for collisional ionization studied with DensMat varied from 1×10^{10} Hz to 1×10^{6} Hz. Step 1 was fixed at 435 834 nm and Step 2 at 470 159 with both lasers being characterized by a spectral bandwidth of 3 GHz. The irradiance at step 1 was 50 W/cm^2 and that for step 2 was 5 kW/cm^2 The transition probability of the first step was taken from tabulated[165] values as 125 MHz while that of step 2 was not known and was therefore assumed to be 5 MHz In addition, a normalized, digitally simulated λ_{23} profile (like that shown in Figure 3-2) was entered into the program as our laser pulse as this excited level had the shortest lifetime in this scheme (~8 ns), and therefore this level determined the temporal performance of the system The only two parameters that were varied were the collisional rate constant and the lifetime of the fourth level (τ_4) The output of DensMat consisted of a plot of fractional level populations *vs* time, which was directly proportional to the output of the oscilloscope current *vs* time. In this way a direct, albeit qualitative, comparison between simulated and experimental results could be made

Results and Discussion

DensMat Simulations

The waveforms generated using DensMat are seen in Figures 3-3a and 3-3b In Figure 3-3a, it is observed that when the collisional ionization rate constant is 10 s^{-1},

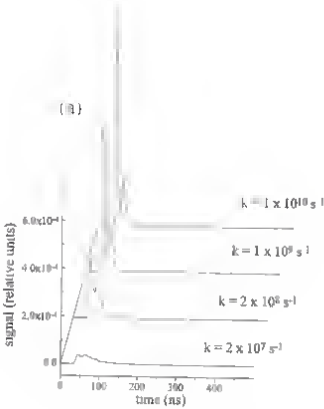

Figure 3 3 DensMat simulation results

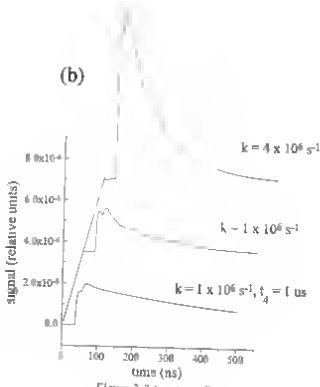

Figure 3-3 (continued).

the signal due to collisional ionization occurs so rapidly that it cannot be distinguished from that due to photoionization. In this case the signal waveform is identical to the λ_{23} pulse. As the rate drops to 1 GHz and then to 0.2 GHz, the signal intensity drops, its temporal behavior broadens and it loses the distinguishing characteristics of λ_{23}. This trend continues for the lower collisional ionization rates presented in Figure 3-3b; it was also observed that increasing the lifetime of level 4 from 200 ns to 1 μs would further broaden this waveform. From these simulations, one can conclude that, as the rate of collisional ionization increases the signal occurs more rapidly for a higher rate (shorter temporal signal) and more slowly for a lower rate (longer temporal signal). The collisional ionization rate can be changed experimentally in two ways: (1) increasing the buffer gas pressure and (2) changing the level from which the collisional ionization occurs, namely, the Rydberg level. From the results of this simulation, it appears that as the principal quantum number of the Rydberg level is increased (i.e., as it becomes closer to the ionization continuum), an increase in the rate of collisional ionization should occur and this increase should be reflected in the ionization waveform in the sense that its shape will increasingly resemble the original waveform of the λ_{23} laser pulse.

Excitation of Levels n = 10 - 14

The first Rydberg levels studied experimentally were n = 10-14. The temporal differences in behavior for these levels are shown in Figure 3-4 (along with the signal from only $\lambda_{12} + \lambda_{23}$, a signal due only to photoionization). The Ar pressure in the cell

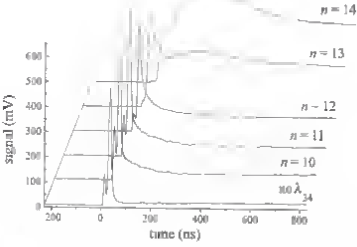

Figure 3-4 Time-resolved waveforms for $n = 10 - 14$

was 70 mTorr and the potential applied between the electrodes was 250 V. The signals were not normalized with respect to laser power.

A trend emerges as one observes levels n = 10 to n = 14. The waveform corresponding to n = 10 resembles the signal with no λ_{34}, with a smaller addition of a longer temporal signal. This second component steadily increased from n = 11 to n = 12 until, at n = 13, it clearly began to dominate. In fact, at n = 14, the photoionization component became almost hidden by the second component. The reasons for this are as follows: at n = 10, the fourth excited level was still too far from the ionization continuum (0.39 eV) for significant collisional ionization to occur at 60 mTorr buffer gas pressure; for this reason, the signal was clearly dominated by photoionization. From n = 11-14, however, a second, longer signal component began to emerge next to that component due to photoionization; the longer signal was a result of collisional ionization. For n = 14, the energy gap to the ionization continuum is only 0.14 eV, and therefore collisional ionization is very significant. Most importantly, the rate of collisional ionization increased with increasing principal quantum number. This trend can be seen even more clearly from the higher-lying levels.

Excitation of Levels n = 18 – 21

The three-step ionization waveforms from Rydberg levels with principal quantum numbers n = 18-21 were also observed. For these levels, the energy gap between the excited level and the ionization continuum became even smaller (0.071 eV for n = 18; 0.049 eV for n = 21), resulting in high rates of collisional ionization. This can be clearly observed in Figure 3-5. The air pressure in the cell was 60 mTorr and the potential

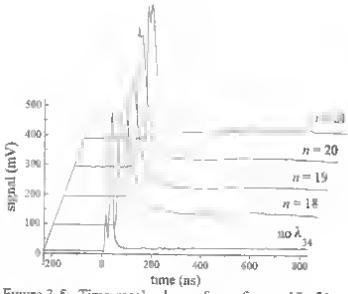

Figure 3-5 Time-resolved waveforms for $n = 18 - 21$

applied between the electrodes was 250 V. The signals were not normalized with respect to laser power. As λ_{34} populated principal quantum numbers from $n = 18$ to $n = 21$, the time duration of the signal shortened due to the increasing rate. What was most striking here was the re-emergence, at $n = 20$, of the laser pulse shape. Although this shape was observed for the lower quantum energy levels ($n = 10$-12) because of the low efficiency of collisional ionization, its reappearance at these high-lying levels was due to an entirely different reason: the rate of collisional ionization was so large that its reciprocal value was much shorter than the duration of the laser pulse. At $n = 21$, collisional ionization was so fast that the waveform resembled that of the exciting laser beam, as a consequence, at these higher levels, deconvolution of the collisional and photoionization components again became difficult. This waveform can be compared to that generated with DensMat for a collisional rate constant of $k = 0.2\ s^{-1}$ (see Fig. 3-3), it is clear that the trend observed as the principal quantum number of the Rydberg level increased follows the trend simulated for increasing the collisional rate constant. As previously stated, we attributed this trend to the collisional ionization component of the signal; the remainder of our work sets out to further prove this hypothesis.

Signal vs. Pressure

The effect of the buffer gas pressure on the collisional ionization signal is shown in Figure 3-6. Here the parameter chosen to show this effect was the full width at half maximum (FWHM), plotted as a function of the pressure of the buffer gas in the cell. The component related to collisional ionization was visually extracted from that due to photoionization. The buffer gas used was Ar; λ_{34} was tuned to $n = 13$ and the potential

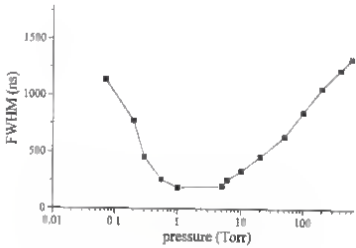

Figure 3-6 FWHM of signal vs pressure.

applied between the electrodes was 240 V. As the pressure increased to about 1 Torr, a decrease in signal duration occurred, showing a minimum around 2 Torr. After that, an increase in signal duration with increasing pressure was again observed. This result further confirmed the source of this component as being due to collisional ionization according to the following explanation. At lower pressures (≤1 Torr), the FWHM depended only on the rate of collisional ionization. On this descending part of the curve, photoionization and collisional ionization could be independently observed as they occurred and could be identified as a function of their rates (photoionization resembles the laser pulse shape and the collisional ionization rate is a function of the Rydberg state excited). At these lower pressures, the rate coefficient for collisional ionization can be expressed as

$$R_c = n_b v \sigma \qquad (3\text{-}1)$$

where R_c is the collisional ionization rate coefficient (s^{-1}), n_b is the concentration of buffer gas (molecules/cm^3), v is the velocity of the buffer gas (cm/s) and σ is the cross-section of collisional ionization (cm^2). Therefore, the collisional ionization rate increased with increasing pressure because of the increase in the concentration of collision partners. From ~5 Torr to ~100 Torr, the FWHM was no longer a function of the collisional rate but instead a function of electron mobility; that is, the time it takes the electrons to travel from the point of ionization to the electrode. At pressures >5 Torr, the FWHM began to increase because of a lower electron drift velocity caused by the increase of buffer gas concentration in the cell. In this pressure range, the collisional ionization and

photoionization signal components were hidden within a longer signal profile which gradually became a function of ion population vs time rather than an observation of the two ionization processes. In this case, since we are dealing with the convolution of both the ion *formation* and *detection* processes, the two components could not be identified or distinguished from each other without difficulty. That is to say, the signal observed was temporally dependent primarily on the electron drift velocity and therefore could not be simply attributed to the ion formation process, like that seen at pressures ≤1 Torr. To increase the velocity of the electrons and again observe the two components separately, a higher potential could have been applied to the electrodes. However, this would have introduced a risk of electrical breakdown and possible damage to the preamplifier. For this reason, this technique was limited to lower potentials and, as a result, to pressures <5 Torr.

The effect of pressure on the ionization signal, at constant collection voltage (250 V) can be further observed in Figure 3-7. In (a), the effect of the buffer gas pressure on the two-step ($\lambda_{13} + \lambda_{23}$, with no λ_{34}) signal is presented. At 60 mTorr, the characteristic laser pulse waveform was observed, indicating that photoionization was dominating. Increasing the pressure to 600 mTorr allowed some collisional ionization to occur, while increasing the pressure to 5 Torr showed a decrease in signal intensity. At 60 Torr, the signal was barely detectable. This behavior was then compared to that of the three-step (λ_{34} added) waveform at $n = 18$, as seen in (b). At 60 mTorr, the collisional ionization signal lasted ~150 ns. When the pressure was increased to 600 mTorr, a much more intense signal occurred lasting about the same amount of time, but with an unexpected longer tail which is difficult to explain. The collisional ionization signal begins to

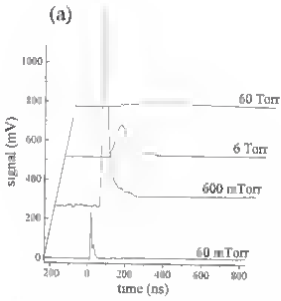

Figure 3-7 Effect of pressure on two-step signal

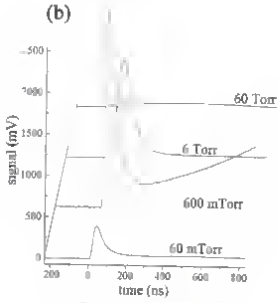

Figure 3-7 (continued).

temporally broaden at 6 Torr until at 60 Torr it is much broader and barely detectable. The same type of behavior as in Figure 3-6 is apparent, however, the observations at n = 18 indicate that the shape of this curve differed for different Rydberg levels.

Signal *vs* Beam Position Between Electrodes

Further proof that collisional ionization was being observed was obtained by monitoring the signal as a function of the overlapping laser beam position between the electrodes. An air pressure of 100 mTorr was used, with 250 V applied between the electrodes, and λ_{34} was tuned to n = 14. As seen in Figure 3-8, the most intense signal was obtained when the beams were directly in front of the high voltage electrode. However, the signal duration remained practically constant and independent of the position of the beams. From this, it could be confirmed that collisional ionization was being observed as it indeed occurred, as any change in the time duration of the waveforms would have indicated that the signal was instead a function of the electron mobility. In other words, if the signal was dependent on the electron mobility or on the configuration of the electric field, then, as the beams were moved away from the high voltage electrode the duration of the signal would have increased due to electron drift.

Signal *vs* Laser Power

In order to support the claim that collisional ionization between the excited atoms and the buffer gas was observed, it was felt that it would be interesting to assess the possible existence of associative ionization. Associative ionization is that contribution to the ionization signal by excited mercury atoms that combine to form ionic dimer

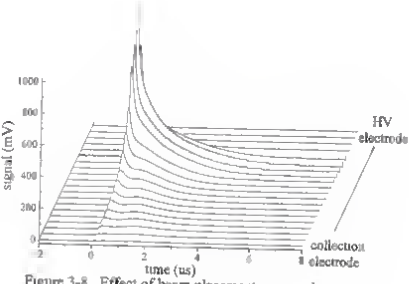

Figure 3-8 Effect of beam placement on signal.

molecules (Hg_2^+). The best way to prove or disprove associative ionization is to change the number density of the excited atoms (Hg^*), as a linear change in the number of excited atoms would affect the change in the number of ionic dimers quadratically. Rather than change the number density of Hg in the cell, the laser power was varied because a linear change in laser power will have a linear effect on the number of excited atoms and therefore a quadratic effect on any associative ions according to the relationship

$$R_a \sim n^* n^* v\sigma \qquad (3\text{-}2)$$

where R_a is the associative ionization rate constant (Hz cm^3), n^* is the concentration of the excited state population ($atoms/cm^3$), v is the velocity of buffer gas (cm/s) and σ is the cross-section of associative ionization (cm^2). While a linear relationship between laser power and ionization signal does not prove associative ionization, it is indicative of a collisional rather than an associative ionization mechanism. As with the location of the overlapping beams, a decrease in laser power of λ_{34} should have no effect on the temporal duration of collisional ionization, while any associative ionization would be affected. The effect can be seen in Figure 3-9 for levels with principal quantum numbers $n = 14$ (Figure 3-9a) and $n = 26$ (Figure 3-9b). In this case, the λ_{23} power was attenuated such that there was no detectable signal from only $\lambda_{12} + \lambda_{23}$; in this way the photoionization source was almost eliminated. An air pressure of 100 mTorr was used with 250 V applied between the electrodes. As can be seen in Figure 3-9, the signal dropped in

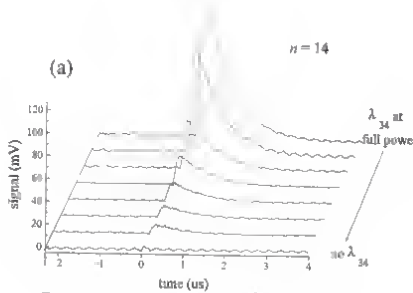

Figure 3-9 Effect of laser attenuation on signal

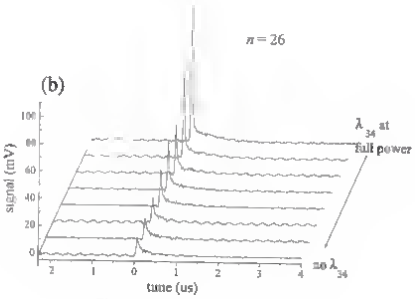

Figure 3-9 (continued)

intensity as the I_{34} power was attenuated, but the temporal behavior and duration remained unchanged. The decrease of the signal intensity with respect to the laser intensity at λ_{34} was linear supporting the claim that the signal was due to collisional ionization. Also, because the duration and shape of the signal did not change it could be assumed that the concentration of species responsible for collisional ionization did not change. This proved that collisional ionization depended on the concentration of buffer gas atoms and/or molecules (as in equation 3-1) and not the excited Hg atoms (as in equation 3-2).

Conclusions

This work has demonstrated the possibility of obtaining simultaneous, and yet separate, information about photoionization and collisional ionization in a *single time-resolved waveform* obtained when Hg atoms are excited in a low pressure gas cell. It has been shown that the signal due to photoionization resembled the laser pulse shape that created it and therefore occurred during the time duration of this pulse while the collisional ionization signal had a longer temporal duration (200-800 ns) depending on the buffer gas pressure and the Rydberg level from which collisional ionization occurred. This experimental evidence agrees with that obtained by simulating the actual conditions with the DensMat model.[164] Observations ranged from $n = 10$, from which little detectable collisional ionization could be observed, to $n = 25$ where collisional ionization occurred so rapidly collisional ionization could not be distinguished from the photoionization component. It was further observed that this type of measurement must

be made at a pressure ≤5 Torr above this pressure the lower electron mobility made it difficult to extract the specific process from the signal From these results, we can conclude that any analytical measurements made using this technique, for a buffer gas at room temperature, must be made at a gas pressure of ≤5 Torr and with ionization from levels n = 10-20 in order to achieve greater selectivity

CHAPTER 4
RESONANCE IONIZATION SPECTROSCOPY OF MERCURY RYDBERG STATES

In order to obtain the best signal-to-noise ratio using RIS, one should directly determine the spectroscopic characteristics of the ionizing atoms, such as the linewidth in a buffer gas and the splitting and shift of the lines in an electric field. It is interesting to note that Rydberg atoms were first studied by observations of the shifts and broadenings that occurred in their spectral lines due to electric field and pressure effects.[166]

Atoms are substantially affected by an applied external field when they are in highly excited or Rydberg, states.[141,166] Here the contribution of Stark effects to the level structure is substantial and sometimes it even represents the dominating contribution. This is because of the large number of closely spaced states, with different orbital angular momentum, which can be easily mixed even in comparatively weak electric fields. In addition, mixing between states can also occur as transitions become unbound. Under these conditions, the selection rules governing the change in parity of states break down, and transitions from states of small values of orbital momentum into those with any value for a given n can occur. In this way, the number of potential spectral lines for an atom increases dramatically.[141] Stark structure observations in Rydberg states have been made for lithium by flame LEI,[167] for calcium by high-resolution laser atomic beam resonance ionization spectroscopy (RIS)[168] and conventional RIS,[169] for aluminum by conventional RIS,[170] and for barium by high resolution RIS.[171]

The broadening and shifting of atomic lines due to collisions with a foreign gas has been studied and reviewed extensively.[17] The main cause of line broadening is the difference of the interaction energies between the radiating atom, in both the initial and final steps of the radiative process, and the colliding atom or molecule. It is a combination of natural broadening, Doppler broadening (which prevails at low pressures) and Lorentz broadening (which dominates at pressures above a few Torr). Collisions of the absorbing atoms with foreign gas molecules induce radiationless transitions and result in a decrease in the lifetime of the excited states. By measuring the half-width of the spectral line, $\Delta\nu_L$, one can calculate the number of collisions experienced per second by an atom. The first measurements of collision properties of Rydberg atoms were carried out by Amaldi and Segre,[173] which unveiled the study of the spectrum of potassium in the presence of noble gases. Techniques used to measure line broadening and shifts include Doppler-free two-photon spectroscopy[174] and the tri-level echo technique.[175]

In this work, the RI spectroscopic characteristics of various Rydberg states for mercury in a buffer gas were studied. A three-step excitation scheme for mercury[162] was used, in which the third step excited the atom to a Rydberg level near the ionization continuum. Measurements were made in a quartz cell containing mercury vapor and buffer gas at varying pressures. Detection occurred via two electrodes, located within the cell, to which a variable high voltage was applied. In this way, the Rydberg lines were observed as a function of electric field and foreign gas pressure, the goal being to find the Rydberg level and the operating conditions which provide the optimal detection of mercury in an analytical RI method.

Although it is known that higher principal quantum number states provide a higher ionization yield, Stark and pressure broadening effects are expected to be more important for some (higher) levels than for others. The sensitivity of the RI method would be decreased by Stark and pressure broadening effects encountered at unnecessarily high principal quantum numbers and excessively high voltages.

A set of conflicting requirements exists with respect to the optimization of the signal to-noise ratio. To saturate the transitions and increase the signal, the power of the laser radiation should be increased. However, in this case, a parasitic signal due to multiphoton ionization of matrix gases could also be present to a greater extent. Due to the strong quenching of Hg excited states which occurs in air under atmospheric conditions, the laser radiation power necessary to saturate the Hg transitions must be increased by at least 100 - 500 times. To decrease the negative effects of quenching and multiphoton ionization one can either decrease the pressure or mix the air containing Hg with Ar (0.1 - 10 Torr) in the cell in which Hg is measured. In this case, the laser power required to achieve saturation can be lowered by 2-3 orders of magnitude. Another contradiction lies in the necessity of measuring the signal using electrodes between which a high voltage must be applied. The electric field can induce Stark splitting and shifts of the levels. This would again require an increase in the laser power in order to achieve saturated transitions.

In view of these considerations, one can see that the development of a method for detecting very low concentrations of mercury atoms in air, liquid, or solid samples using the RI method requires the optimization of a significant number of parameters. By studying the spectral characteristics of the Rydberg levels, we can identify the optimal

level to be reached in the RI excitation scheme as well as the pressure and voltage which should be used to attain the maximum sensitivity and the ultimate limit of detection

Experimental

The experimental setup used in this work is similar to the one described in previous chapter (Figure 3-1) The calculated wavelengths and corresponding energies of the three dye laser-connected transitions are listed in Table 4-1 In this table the expected transitions as tabulated by Moore[163] and Barg[176] and as observed in this work are listed The data tabulated by Moore was collected from reports dating up to 1955 Only principal quantum numbers up to $n = 26$ were observed at that time The transitions observed by Barg in 1983 extend up to $n = 37$ for the $np\ ^1P_1{}^0$ series and $n = 48$ for the $np\ ^3P_1{}^0$ series, but there is no reported observation of the $np\ ^3P_2{}^0$ series.

The wavelengths observed in this work have an uncertainty of ±5 pm due to the bandwidth of the laser This corresponds to an uncertainty of ±0.5 cm^{-1} in the calculated energy level

The beams were directed with mirrors and prisms into a quartz cell which contained a small amount of mercury and varying pressures of buffer gas (air or argon) At atmospheric pressure, the Hg number density in the cell was ~ 4×10^{13} cm^{-3} The cell also housed two planar Ni electrodes and was connected to a vacuum pump and to an argon supply, which allowed varying pressures (100 mTorr – 800 Torr) of argon into the cell Due to the poor performance of the vacuum system at low pressures, the composition of gas in the cell at the lowest attainable pressures (~75 mTorr) was air

Table 4-1 Excitation transitions for Hg for laser-connected levels 1 2 3 and 4 (Rydberg level) as tabulated by Moore,[163] Baig,[178] and in this work for $n = 6, 7-10-48$

Excitation Step	Level	Energy, cm^{-1} Moore	Energy, cm^{-1} Baig	Energy, cm^{-1} this work	Wavelength in air, nm Moore	Wavelength in air, nm Baig	Wavelength in air, nm this work
λ_{12}	$6p^3P_1^o$	39412.3	39412.39	—	253.652	253.652	—
λ_{23}	$7s^3S_1$	62350.5	—	—	435.832	—	—
λ_{34}	$10p^3P_0^o$	80902.27	—	—	538.882	—	—
	$10p^3P_1^o$	80916.686	80916.17	80917.6	538.463	538.437	538.436
	$10p^3P_2^o$	81022.9	—	81022.7	535.408	—	535.406
	$10p\ ^1P_1^o$	81153.614	81153.09	81154.3	531.677	531.692	531.657
	$11p^3P_0^o$	81800.0	—	81800.7	514.007	—	513.988
	$11p^3P_1^o$	81811.876	81807.55	81808.3	513.693	513.808	513.789
	$11p^3P_2^o$	81873.835	—	81873.7	512.063	—	512.065
	$11p^1P_1^o$	81942.444	81941.89	81942.4	510.270	510.283	510.271
	$12p^3P_0^o$	—	—	82374.6	—	—	499.258
	$12p^3P_1^o$	82379.0	82378.09	82378.9	499.150	499.172	499.151
	$12p^3P_2^o$	82422.80	—	82422.8	498.064	—	498.061
	$12p^1P_1^o$	82464.05	82463.48	82464.3	497.038	497.052	497.032
	$13p^3P_1^o$	82765.9	82765.43	82772.3	489.689	489.701	489.535
	$13p^3P_2^o$	82795.03	—	82800.3	488.991	—	488.865
	$13p^1P_1^o$	82823.84	82823.55	82825.1	488.301	488.310	488.273
	$14p^3P_1^o$	83039.3	83040.20	83041.2	483.219	483.198	483.175
	$14p^3P_2^o$	83061.2	—	83063.7	482.708	—	482.651
	$14p\ ^1P_1^o$	83084.0	83081.60	83083.1	482.177	482.233	482.199
	$15p^3P_1^o$	83240.1	83242.25	83242.9	478.573	478.524	478.510
	$15p^3P_2^o$	83258.7	—	83260.2	478.147	—	478.114
	$15p\ ^1P_1^o$	83280.5	83272.96	83273.6	477.649	477.821	477.806
	$16p^3P_1^o$	83396.7	83394.98	83395.9	475.011	475.050	475.030
	$16p^3P_2^o$	83407.2	—	83409.2	474.776	—	474.731
	$16p\ ^1P_1^o$	83420.3	83418.21	83419.3	474.481	474.528	474.503
	$17p^3P_1^o$	83512.7	83513.31	83514.4	472.409	472.395	472.371
	$17p^3P_2^o$	83521.6	—	83524.8	472.210	—	472.138
	$17p^1P_1^o$	83530.7	83531.65	83532.7	472.007	471.986	471.963
	$18p^3P_1^o$	83601.9	83687.15	83607.9	470.425	470.309	470.292
	$18p^3P_2^o$	83613.9	—	83616.4	470.160	—	470.105
	$18p\ ^1P_1^o$	83619.9	83621.62	83622.5	470.027	469.989	469.969
	$19p^3P_1^o$	83677.9	83682.36	83683.7	468.748	468.650	468.621
	$19p^1P_1^o$	83686.0	—	83690.3	468.570	—	468.476

Table 4-I continued

Excitation Step	Level	Energy cm^{-1} Moore	Energy, cm^{-1} Baig	Energy cm^{-1} this work	Wavelength in air nm Moore	Wavelength in air, nm Baig	Wavelength in air nm this work
	$19p\ ^3P_1^o$	83691.3	83693.92	83695.3	468.454	468.396	468.366
	$20p\ ^3P_1^o$	—	83743.68	83699.5	—	467.306	468.275
	$20p\ ^1P_1^o$	83745.7	—	83750.6	467.263	—	467.156
	$20p\ ^3P_1^o$	—	83753.50	83754.7	—	467.092	467.067
	$21s^3P_1^o$	—	83794.41	83795.9	—	466.201	466.169
	$21p^3P_2^o$	83792.8	—	83800.5	466.236	—	466.068
	$21p^3P_1^o$	—	83802.49	83803.9	—	464.025	465.994
	$22p^3P_1^o$	—	83837.13	83838.2	—	465.274	465.251
	$22p^3P_2^o$	83834.5	—	83842.0	463.331	—	465.168
	$22p\ ^1P_1^o$	—	83843.73	83844.9	—	465.131	465.105
	$23s^3P_1^o$	—	83873.06	83874.3	—	464.500	464.473
	$23p^3P_2^o$	83868.0	—	83871.6	464.609	—	464.402
	$23p^3P_1^o$	—	83878.61	83880.1	—	464.380	464.348
	$24p^3P_2^o$	—	83903.74	83904.9	—	463.838	463.813
	$24p^3P_1^o$	83892.6	—	83907.7	464.078	—	463.753
	$24p^1P_1^o$	—	83908.46	83909.9	—	463.737	463.706
	$25p^3P_1^o$	—	83930.01	83931.3	—	463.274	462.246
	$25p^3P_2^o$	83920.8	—	83933.7	463.471	—	463.195
	$25p\ ^1P_1^o$	—	83934.09	83935.5	—	462.186	463.155
	$26p^3P_1^o$	—	83952.84	83954.0	—	462.784	462.760
	$26p^3P_2^o$	83942.0	—	83956.0	463.016	—	462.716
	$26p^1P_1^o$	—	83956.57	83957.7	—	462.704	462.679
	$27p^3P_1^o$	—	83972.43	83973.8	—	462.364	462.335
	$27p^3P_2^o$	—	—	83975.6	—	—	462.297
	$27p^1P_1^o$	—	83975.75	83977.2	—	462.293	462.263
	$28p^3P_1^o$	—	83989.83	83991.4	—	461.992	461.960
	$28p^3P_2^o$	—	—	83992.8	—	—	461.929
	$28p\ ^1P_1^o$	—	83992.75	83994.4	—	461.930	461.896
	$29p^3P_1^o$	—	84005.24	84006.5	—	461.664	461.636
	$29p^3P_2^o$	—	—	84007.8	—	—	461.609
	$29p^1P_1^o$	—	84007.85	84009.2	—	461.608	461.579
	$30p^3P_1^o$	—	84018.72	84020.1	—	461.376	461.348
	$30p^3P_2^o$	—	—	84021.1	—	—	461.325
	$30p\ ^1P_1^o$	—	84020.68	84022.5	—	461.328	461.296
	$31p^3P_1^o$	—	84031.07	84032.2	—	461.113	461.090
	$31p^3P_2^o$	—	—	84033.0	—	—	461.072

Table 4-I continued

Excitation Step	Level	Energy, cm^{-1} Moore	Energy, cm^{-1} Baig	Energy, cm^{-1} this work	Wavelength in air nm Moore	Wavelength in air nm Baig	Wavelength in air nm this work
	$31p\ ^3P_2^o$	—	84032.84	84034.5	—	461.076	461.041
	$32p\ ^3P_1^o$	—	84041.88	84043.0	—	460.884	460.860
	$32p\ ^3P_2^o$	—	—	84043.7	—	—	460.845
	$32p\ ^1P_1^o$	—	84043.50	84045.2	—	460.849	460.814
	$33p\ ^3P_1^o$	—	84051.34	84052.6	—	460.683	460.656
	$33p\ ^3P_2^o$	—	84053.11	—	—	460.645	—
	$34p\ ^3P_2^o$	—	84060.10	84061.2	—	460.497	460.474
	$34p\ ^1P_1^o$	—	84061.46	—	—	460.464	—
	$35p\ ^3P_1^o$	—	84068.02	—	—	460.329	—
	$35p\ ^3P_2^o$	—	84069.58	—	—	460.297	—
	$36p\ ^3P_1^o$	—	84075.23	—	—	460.176	—
	$36p\ ^3P_2^o$	—	84076.57	—	—	460.148	—
	$37p\ ^3P_1^o$	—	84081.94	—	—	460.034	—
	$37p\ ^3P_2^o$	—	84083.00	—	—	460.011	—
	$38p\ ^3P_1^o$	—	84087.95	—	—	459.907	—
	$39p\ ^3P_1^o$	—	84093.33	—	—	459.793	—
	$40p\ ^3P_1^o$	—	84098.21	—	—	459.690	—
	$41p\ ^3P_1^o$	—	84102.88	—	—	459.593	—
	$42p\ ^3P_1^o$	—	84107.12	—	—	459.501	—
	$43p\ ^3P_1^o$	—	84111.15	—	—	459.416	—
	$44p\ ^3P_1^o$	—	84114.76	—	—	459.340	—
	$45p\ ^3P_1^o$	—	84118.09	—	—	459.278	—
	$46p\ ^3P_1^o$	—	84121.20	—	—	459.204	—
	$47p\ ^3P_1^o$	—	84124.10	—	—	459.143	—
	$48p\ ^3P_1^o$	—	84126.79	—	—	459.086	—

[a] uncertainty in wavelength ±0.005 nm, corresponding to ±0.5 cm^{-1} uncertainty in energy

rather than argon. One electrode was connected to a high voltage source which applied varying potentials (0 - 1.5 kV) to the cell, while the other was connected to a low-noise charge sensitive preamplifier (Avangard Inc., Russia). The amplified signal was averaged using a boxcar averager (Model SR560, Stanford Research Systems, Sunnyvale CA) and recorded on a laptop computer. In addition, the amplified RI waveform was displayed on a fast digitizing oscilloscope (Model 620A, Tektronix, Beaverton, OR).

Results and Discussion

Assigning Spectral Lines

In order to observe the spectral lines that were being excited from the second excited level by the third laser connected step, λ_{34} was scanned over the range 455 - 539 nm. The air pressure in the cell was 100 mTorr and the voltage applied between the electrodes was 40 V. A series of lines was observed emerging from the continuum (calculated as 457.7 nm), which became more spread out with increasing wavelengths. Each principal quantum number was observed as three lines; these lines were more resolved at lower n and began to merge together as the lines approached the continuum, as seen in Figure 4-1. Lines with principal quantum number up to $n = 42$ were observed (with an applied voltage of 40 V) before the lines merged into the continuum. Only those lines up to $n = 34$ were assigned (as seen in Table 4-1) due to the merging of the triplet observed as the continuum is approached. Inset (i) shows the lines closest to the continuum ($n \geq 32$). After observing the spectrum as a function of the λ_{34} laser power, it

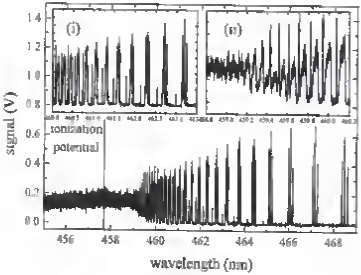

Figure 4-1 Spectrum of Hg Rydberg States

was clear that none of these levels were saturated. When observing the triplets shown in Figure 4-1, one might expect these lines to be attributed to the $7^2S_1 \rightarrow np\ ^3P_{0,1}{}^0\ ^3P_1{}^0$ and $^3P_2{}^0$ transitions. However further studying of these lines showed that they can be attributed from blue to red as $^1P_1{}^0\ ^3P_2{}^0,\ ^3P_1{}^0$. At an air pressure of 75 mTorr and with 350 V applied between the electrodes, the $7^2S_1 \rightarrow np\ ^3P_0{}^0$ transition was observed as very weak lines only for n = 10, 11, and 12 (n = 12 is shown in Figure 4-2). In this way, all allowed transitions were observed, including those with n values previously not tabulated.

The wavelengths observed in this work correspond more closely with those of Barg,[76] especially those above n = 14, than those of Moore.[60] Although Barg reports no values for the $np\ ^3P_2{}^0$ levels, the trend observed for the $np\ ^1P_1{}^0$ and $np\ ^3P_1{}^0$ series is the same as that observed in this work for all three series, with calculated wavelengths within 30 pm of those observed by Barg.

In addition to these lines, another series appeared between 460.0 - 463.5 nm as seen in Figure 4-1(ii). These lines do not correlate with the triplets which correspond to each principal quantum number. One possible explanation for the appearance of these lines is that they correspond to a normally forbidden transition occurring for very high n values, when the mixing of Rydberg states can occur even for weak electric fields.[41]

Stark Effects

The Stark effect causes splitting, shifting, and mixing of high-lying Rydberg states with increasing electric field. This rather pronounced effect can be observed for n = 14 with 60 mTorr of air in Figure 4-3. A nondisturbed spectral line shape is observed for

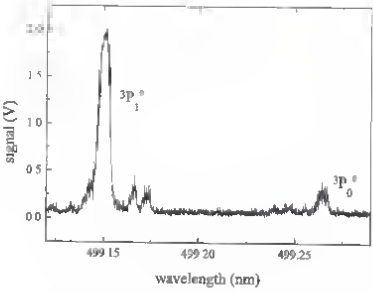

Figure 4-2 Spectral lines attributed to 12 $^3P_1{}^0$ and $^3P_0{}^0$

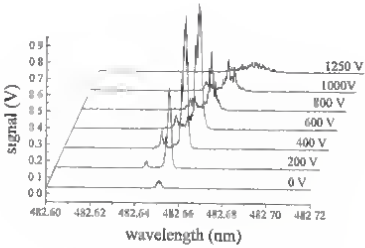

Figure 4-3. Effect of high voltage on $n = 14$ (Stark effect)

applied voltages of 400 - 600 V. However, at higher voltages (up to 1250 V), the peak becomes significantly broadened and some shifting is observed.

However, the Stark effects at $n = 14$ can be considered negligible compared to those that occur for higher lying Rydberg states. Because the orbital radius of the Rydberg electron increases with n^2 and the binding energy decreases with $1/n^2$, Stark effects become more dominant with increasing n. For higher n levels, the electron is more easily coupled to the electric field. This can be observed in Figure 4-4, which compares the spectra for $n = 25$, 26, and 27 at 300 mTorr of air, for applied voltages of 200 V and 365 V. In both cases, the difference in the electric field had a visible effect on the spectral line shapes. For all three n values, the $^3P_1^0$ and $^3P_2^0$ lines broaden with increased voltage. However, the most pronounced Stark effects are observed for the $^1P_1^0$ state, which appears to experience both splitting and broadening, to the extent that it merges into the $^3P_2^0$ state.

At $n \geq 30$, the most pronounced influence of the Stark effect is the mixing of the three observed states, as seen in Figure 4-1(*f*). Even at low applied voltages (~ 40 V), the mixing becomes so efficient (especially the singlet state with the nearby $^3P_2^0$) that it is impossible to deconvolute one state from another at ~ $n = 32$. For these higher levels, it is also impossible to compare different voltages to observe broadening, as broadening is occurring even at the lowest voltages necessary for electrical detection. This broadening is not only a result of Stark effects, but also a result of the breakdown of well-defined states that exist near the continuum. At some point, the highly excited Rydberg electron is residing in states that can no longer be defined as bound states, this is another reason for the mixing of states.

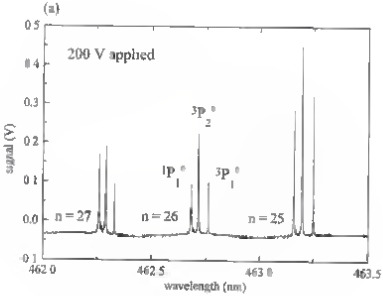

Figure 4-4 Spectrum of $n = 25, 26, 27$

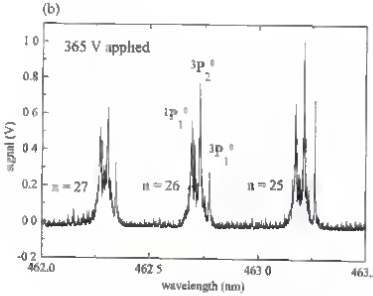

Figure 4-4 (continued).

Buffer Gas Pressure Shifts and Broadenings

An increase in pressure can cause both a broadening and a shifting of the mercury Rydberg states, as can be seen for $n = 10$ in Figure 4-5 with 200 V applied between the electrodes. In addition to these pressure effects which occur to varying degrees for all spectral lines, some spectral lines also experience increasing asymmetry (as seen in Figure 4-5) and even the appearance of new spectral features at higher pressures. Unlike Stark effects, the broadening and shifting of spectral lines do not increase with n with increasing pressure. However, for low-lying Rydberg states ($n < 10$), these effects do in fact increase with pressure. As the orbital radius increases, so does the Rydberg atom's interaction sphere and thereby the probability of a collision with a perturber. However, at higher-lying states, the Rydberg electron is so far from the ionic core of the atom that the atom becomes "transparent" to collision partners and the probability of interaction decreases and even approaches zero.[158] For this reason, a maximum in line width is observed with increasing n for higher pressures; this maximum is predicted to occur around $n \sim 10$. This was observed to occur in the case of mercury, after this was observed, measurements for $n \geq 10$ were made with 100 V applied between the electrodes, as seen in Figure 4-6.

For both $^3P_2^0$ (Fig. 4-6a) and $^3P_1^0$ (Fig. 4-6b), the linewidth decreases for principal quantum numbers between $n = 10$ and $n = 15$ and reaches a plateau for higher n values. For the $^3P_2^0$ states a symmetrical line appears with changing halfwidth for each n until the merging of the three states makes it impossible to define the true halfwidth of each individual state. For the $^3P_1^0$ states not only does the line for each n become broader with increasing pressure, but it also becomes asymmetrical, with some tailing to the red

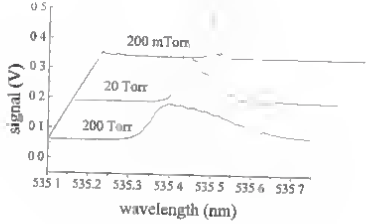

Figure 4-5 Effect of pressure on $n = 10$

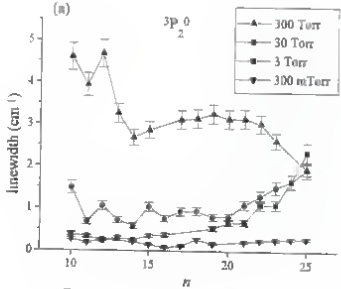

Figure 4-6 Linewidth vs. n

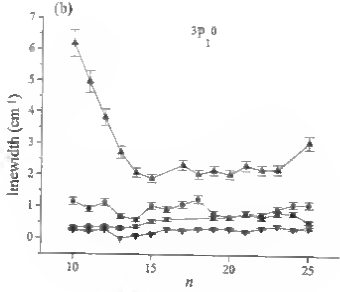

Figure 4-6 (continued)

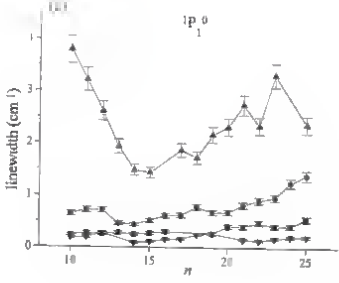

Figure 4-6 (continued)

For the $^1P^6$ states (Fig. 4-6c) the same trend in line broadening with increasing n is observed but with no plateau. For this state new spectral features which increase with increasing pressure are observed, in addition to an asymmetry similar to that found for $^3P_1^6$. From this, as from the exaggerated Stark effects on this transition as compared to the triplet states, it is clear that the $^1P_1^6$ is more easily perturbed by outside influences than the $^3P_{1,2}^6$ states. This occurs because the parallel spins of the two mercury valence electrons (one in Rydberg state and one in its ground state) of the triplet state remain more bound than the paired spins of the two electrons in the singlet state. Thus lack of a bound relationship to the valence electron closer to the ionic core makes the singlet state Rydberg electron more susceptible to outside influences.

Conclusions

In this work, several excitation schemes of Rydberg states for Hg have been presented and assigned. The effect of higher pressures of the buffer gas on the structure of the Rydberg levels was found to be significant. In addition, this effect was observed to be greatest for $n = 10$; for larger values of n the effect became less pronounced. The applied electric field (Stark effect) was observed to become increasingly influential on the level structure with increasing principal quantum number and was most pronounced for $n > 14$. By studying the spectral characteristics of Hg Rydberg levels one can choose the optimal excitation level and operating conditions for obtaining the best analytical sensitivity and limit of detection available by RIS for Hg. From the results shown here it appears that the optimal results for the detection of Hg in a buffer gas are obtained by

exciting $n = 10$ 14 at the lowest possible pressure of buffer gas (~60 mTorr) with a high voltage of no more than 250 V applied between the electrodes.

CHAPTER 5
RESONANCE IONIZATION OF MERCURY ATOMS IN AN INERT ATMOSPHERE WITH AVALANCHE AMPLIFICATION OF THE SIGNAL

It has been shown[140,141] that, under certain experimental conditions, resonance ionization methods are capable of detecting single atoms in an atmosphere of inert gas or under vacuum. When detecting atoms with ionization techniques in real samples using standard analytical methods for sample atomization (e.g. flames, plasmas, furnaces, or a combination of them) the detection limit depends on the background caused by the number of charged particles in the volume illuminated by laser radiation (the interaction region). For the most part, these particles are created as a result of nonselective laser ionization and thermal ionization of buffer gas or matrix atoms/molecules.[137-40] One way to eliminate thermal ionization is to use cold atomization of the sample.

This method is commonly used for the atomization of mercury and is known as cold vapor generation. It involves reducing inorganic Hg in solution to its elemental form and purging the solution with an inert gas. In this way, a stream of inert gas containing the Hg atoms is carried to the detection cell. It was first reported as an atomization source for atomic absorption spectrometry by Hatch and Ott[16] for determination of Hg in water samples. For other elements that are not as volatile at room temperature (including As, Bi, Ge, In, Pb, Sb, Se, Sn, Te, and Tl), the method of hydride generation is widely used to form gaseous analytes.[141]

In addition to cold vapor generation there are several other methods which involve cold atomization. For example, the sample can be evaporated in a low temperature atomizer or by pulsed or CW laser radiation and the resulting vapor selectively ionized and detected.[182] Using a glow discharge, created by a fast electrical pulse, nonselectively ionized particles can be rapidly removed and the analyte again selectively ionized and detected in a background-free buffer gas.[183]

Compared to other methods, cold atomization can be advantageous in combination with laser ionization spectroscopy techniques as it can lead to a dramatic improvement of the detection limit of the atoms probed by the laser(s), and consequently of those present in the original sample. This is due to (1) the elimination of charged background particles due to thermal ionization, (2) the feasibility of an avalanche effect in the buffer gas, which increases the signal by several orders of magnitude [150] and (3) the fact that because the spectral lines are narrower, less energy is required to saturate transitions at low temperatures. The third advantage is important because low laser irradiance potentially decreases the probability of multiphoton ionization processes in the buffer gas and the resulting high background levels. For these reasons, counting atoms in real samples using cold atomization becomes a real possibility.

The first step in realizing this goal must be the determination of optimal conditions for collisional ionization and photoionization while minimizing the background due to nonselective multiphoton ionization. At the same time, conditions to achieve the optimal avalanche amplification of the signal while retaining proportionality between the signal and the number of atoms in the interaction region, must be found.

The aim of this work was to find these optimal conditions as well as the optimal excitation transitions, laser energy and electric field which would allow one to reach the ultimate detection limit for mercury atoms in an inert, gaseous environment at ambient temperature.

Experimental

The experimental setup used in this work, shown in Figure 5-1 for the sake of clarity, is similar to the one described Chapters 3 and 4. The transitions to be studied, as tabulated by Moore,[163] are listed in Table 5-1. The corresponding wavelengths (in air) of the three laser-connected steps were calculated from these transitions.

The beams were directed with mirrors and prisms into the sample cell. This cell is shown in Figure 5-2 in its two detection configurations. The cell itself was a 15-cm long, 1 cm i.d. fused silica tube plugged at the top with a ceramic stopper, through which a 2 mm hole was bored vertically through the center. The fused silica tube was connected to an Ar or P-10 gas (90% Ar, 10% CH_4) tank with a small fused silica reservoir in between. This reservoir contained a small amount of elemental Hg. In this way, inert gas was passed over the liquid Hg at flow rates of 1-100 *ml/min*, picking up Hg atoms in the vapor phase and carrying them through the detection cell. An additional gas line was connected to the output of the Hg reservoir in order to allow dilution of the Hg atoms in the inert gas flow. The laser beams passed through the cell *via* a 2 mm hole bored horizontally through the ceramic stopper (Fig. 5-2a) or above the stopper, with the horizontal hole covered to prevent loss of analyte (Fig. 5-2b). When the Hg-containing

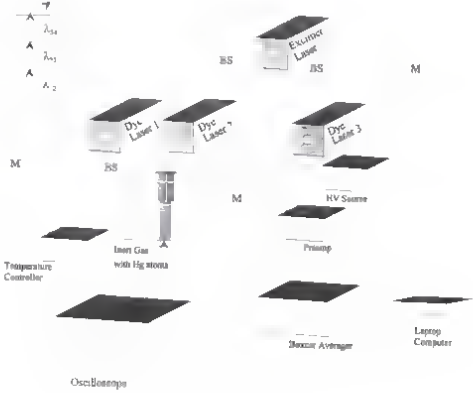

Figure 5 1 Experimental setup

Table 5-1 Excitation transitions for Hg for laser-connected levels 1, 2, 3, and 4 (Rydberg level), as tabulated by Moore,[165] for $n = 6,7,9\text{-}13$

Excitation step	Level	Energy, cm^{-1}	Wavelength in air, nm
λ_{12}	$6p^3P_1^0$	39412.3	253.652
λ_{23}	$7s^3S_1$	62350.5	435.832
λ_{34}	$9\,p^3P_2^0$	79412.7	585.925
	$9\,p^3P_1^0$	79613.3	579.118
	$10p^3P_0^0$	80902.27	538.880
	$10p^3P_1^0$	80916.7	538.463
	$10p^3P_2^0$	81022.9	535.400
	$10p^1P_1^0$	81153.6	531.678
	$11p^3P_0^0$	81800.0	514.012
	$11p^3P_1^0$	81811.9	513.694
	$11p^3P_2^0$	81873.8	512.064
	$11p^1P_1^0$	81942.4	510.270
	$12p^3P_0^0$	82379.0	499.148
	$12p^3P_2^0$	82422.6	498.064
	$12p^3P_1^0$	82464.1	497.037
	$13p^3P_1^0$	82765.9	489.689
	$13p^3P_2^0$	82795.0	488.991
	$13p^1P_1^0$	82823.9	488.300

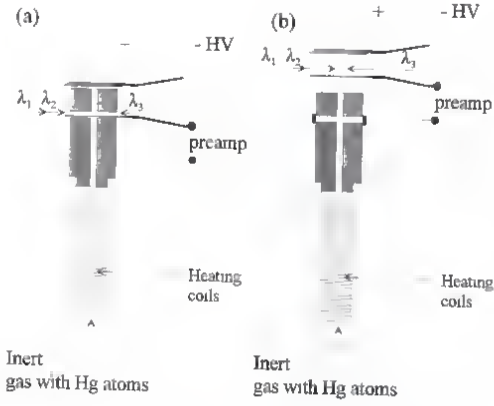

Figure 5.2 Detection cell: two electrode configurations.

inert gas reached this point, the Hg atoms were selectively ionized and the resulting charges detected by a pair of electrodes

A planar Ni electrode was connected to a high voltage source which applied varying potentials (0 - 3 kV) between the planar electrode and a 0.1 mm diameter W wire electrode which was connected to a low-noise charge sensitive preamplifier (Avangard, Inc., Russia). The amplified signal was processed using a boxcar averager (Model SR560, Stanford Research Systems, Sunnyvale, CA) and recorded on a laptop computer. In addition, the amplified ionization waveform was displayed on a fast digitizing oscilloscope (Model 620A, Tektronix Beaverton, OR).

In order to apply heat to the cell, a heating coil was wrapped around the cell and connected to a variable voltage transformer. Insulating tape was wrapped around the heating coil. With this system, temperatures up to 550 K could be obtained in the gas volume which was irradiated by the laser. It is important to note that an increase in temperature was not applied to the Hg reservoir since our aim was not that of varying the amount of mercury passing through the cell but rather to increase the number of collisions of the same number of Hg atoms.

In order to attenuate the laser energy of the third laser step, a variable neutral density filter wheel was placed in front of λ_{34}. The wheel was calibrated for λ_{34} before use.

Results and Discussion

Signal vs Temperature

The ionization signal was first studied as a function of temperature in an attempt to increase the rate of collisional ionization. In the resonance ionization literature,[104] it is well known that the two factors influencing the rate of collisional ionization are (1) the energy difference between the excited atomic levels of different principal quantum number (from which ionization is occurring) and the ionization continuum and (2) the number of ionizing collisions, which depends on the temperature in and around the interaction region. The former factor was studied in Chapter 3, in which we observed the behavior of the rate of collisional ionization when different atomic levels, of increasing principal quantum number, were reached by laser excitation.

For the present experiments, the electrode configuration presented in Fig. 5-2b was initially tested. However, a significant loss of signal at higher temperatures was encountered with this setup. These losses were attributed to the quenching of the Hg excited states as a result of the atoms being exposed to air and water vapor molecules. For this reason, the configuration of Fig. 5-2a was used for all subsequent temperature measurements in order to keep the Hg in as inert an atmosphere as possible.

The signal was measured at two temperatures (~300 K and ~550 K) and for several different final excitation steps (λ_{34}) corresponding to different 7s - np $^3P_2^0$ transitions with n varying from 9 to 13 (see Table 1). In an attempt to differentiate between the mechanisms of photoionization and collisional ionization, the behavior of the

signals at these two temperatures as a function of λ_{34} laser energy was investigated by using the variable neutral density filter wheel to attenuate the laser energy. The results for $n = 10$ ($\lambda_{34} = 535.400$) are shown in Figure 5-3. Clearly, at these temperatures and laser energies, no indication of signal saturation due to the attainment of maximum ionization rates is yet observed. Indeed, even after increasing the energy of the third laser step to values between 700-900 μJ, the data (not reported in Fig. 5-3) did not show a plateau. In addition, at any given value of laser energy, no remarkable difference in the magnitude of the signal, for the two temperatures in the figure, can be seen. Similar behavior was observed for $n = 11$ and $n = 12$.

The dependence of the behavior of the ionization signal on temperature at lower laser irradiances is seen in Figure 5-4 for $n = 10$, 11, and 12. In this case, a fixed laser energy for λ_{34} of 0.1 mJ was used with a beam that was less tightly focused than for the data shown in Fig. 5-3; therefore, no direct comparison between the two figures should be made. In all the cases shown in Figures 5-3 and 5-4, the signals were normalized for thermal expansion. For $n = 10$, a moderate increase in signal was achieved with increasing temperature, while a more significant dependence was seen for $n = 11$. On the contrary, for $n = 12$, the signal showed almost no dependence on temperature, and even a slight decrease at higher temperatures.

Although a quantitative explanation of the above results is not possible on the basis of the few data available, a qualitative interpretation can be attempted on the following grounds. First of all, it is reasonable to assume that, for $n = 10$ and at high laser energies, photoionization rather than collisional ionization is the dominating mechanism of the production of charges (see Fig. 5-3). There is no doubt that collisions from the

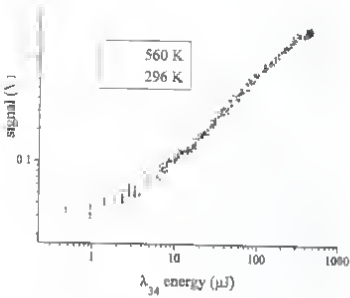

Figure 5-3 Signal vs λ_{34} energy, $n = 10$

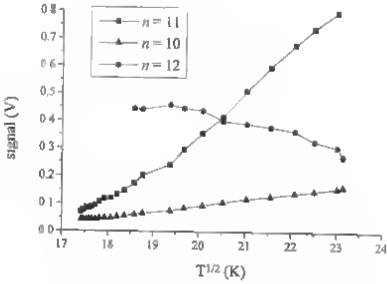

Figure 5-4 Signal vs temperature for $n = 10, 11, 12$.

final excited level contribute to the signal but, at these temperatures and laser energies, this contribution is negligible compared to photoionization.

The different behavior of levels $n = 10$, 11, and 12 with temperature seen in Fig. 5-4 can be attributed to a complex interplay between several parameters such as energy difference with the ionization continuum and non-ionizing, quenching collisions, which have opposite effects on the magnitude of the signal. For $n = 10$, 11, and 12 it appears that quenching, collisional ionization and photoionization are all contributing, but our present data do not allow us to extract individual contributions to the overall signal. For the data presented in Fig. 5-4 where a less focused laser was used, photoionization probably plays only a small role. The significant increase in ionization which is observed in going from $n = 10$ to $n = 12$ (at low temperatures) further supports this conclusion. To summarize these speculations, with lower laser irradiance, one can assume that collisional ionization is the dominant ionization process for $n = 10$ and 11 and the larger number of collisions at increasing temperatures results in an increasing signal, while for $n = 12$, quenching may dominate over the other processes at higher temperatures.

In view of the fact that, at low temperatures, the signal observed for $n = 12$ was the largest, and also because in this case λ_{3d} (498.064 nm) lies at the peak of the gain curve of the dye, this Rydberg level was used in all subsequent experiments.

Avalanche Amplification

The experiments for optimizing the avalanche amplification of the signal employed the electrode configuration shown in Fig. 5-2b because the configuration in Fig. 5-2a resulted in noise and an electrical breakdown occurring between the two

electrodes which could result in destruction of the preamplifier. With the configuration in Fig. 5-2b, voltages of up to 3 kV could be used without any onset of electrical breakdown occurring.

The avalanche amplification studies were carried out with an inert gas flow of < 2 mL/min. In addition, an extra line of Ar gas was introduced to the cell to further dilute the number of Hg atoms and reduce space charge effects.

The first avalanche amplification studies involved the use of Ar as the inert gas. The results of this study are shown in Figure 5-5. This figure shows the classical behavior of an avalanche effect,[185,186] i.e., the signal remains relatively constant until it reaches a threshold level where an avalanche amplification, which is linearly related to the initial number of charges created, begins to appear. This behavior remains linear until it starts to be affected by the onset of some other behavior, such as space charge effects due to the presence of a large number of electrons between the electrodes or electrical breakdown. However, Ar resulted in an amplification factor of only 50 before electrical breakdown occurred. In order to increase the amplification factor, Ar was replaced with P-10 gas (90% Ar, 10% CH_4).

The results of the study using P-10 gas are shown in Figure 5-6. In curve 1, the avalanche amplification obtained with three laser-connected steps is shown. Typical behavior was seen up to a high voltage of ~2000 V. At this point, space charge effects began to dominate and the proportionality with the initial number of charges was lost.[186,188] In order to avoid these effects, for applied high voltages above 2000 V, the ionization signals generated using only the first two laser-connected steps were observed. The voltage dependence of this signal is shown in curve 2 and has been normalized to the

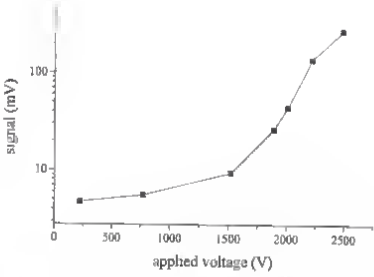

Figure 5-5 Avalanche amplfication of the signal using Ar

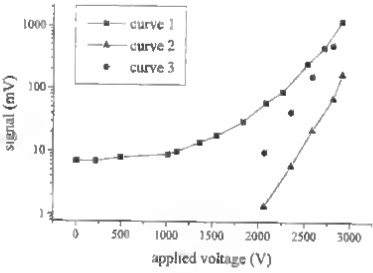

Figure 5-6 Avalanche amplification of the signal using P-10 gas

3-step results in curve 3. In this way the influence of space charge effects was avoided and the expected sharp rise in the signal with high voltage, due to the avalanche effect, was restored. The amplification factor for the HV region where three steps could be utilized was 7.5, and the remainder of the amplification, achieved with just the two steps was 12.1. This results in a total amplification factor of 7.5 × 12.1 or 90.6.

In order to insure that the avalanche amplified signal was related to the initial number of charges created as a result of the ionization of Hg atoms in the laser irradiated volume, a spectral scan of the second laser step was performed at applied high voltages of 0.5 kV and 2.7 kV for the electrode configuration shown in Fig. 5-2a, and of 3 kV for the configuration in Fig. 5-2b. These results are shown in Figure 5.7. When comparing Figures 5-7b and 5-7c, it is clear that the second electrode configuration (Fig. 5-2b) not only prevented electrical breakdown from occurring, but also resulted in a decrease of the random fluctuations of the signal observed at high voltages. The smoothed and normalized spectral profiles for λ_{23} are shown in Figure 5.8. The close resemblance between the spectral shapes of the avalanche amplified signal and the signal observed at low voltages (where no avalanche amplification occurs) is a clear indication that the former signal carried the same direct proportionality with the initial number of charges (i.e., Hg atoms) created as did the latter.

Limit of Detection

The overall efficiency of ionization (collisional + photo) for the different excited Rydberg levels (n = 10, 11 and 12), η_{ny}, can be estimated from the magnitude of the

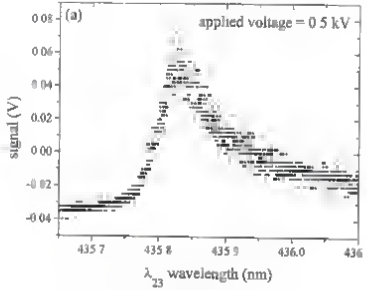

Figure 5-7 Spectral profile of λ_{23}

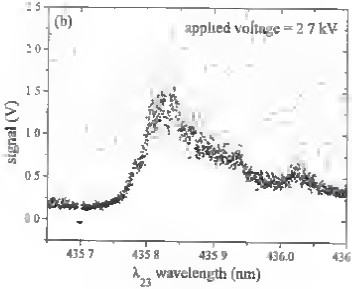

Figure 5-7 (continued)

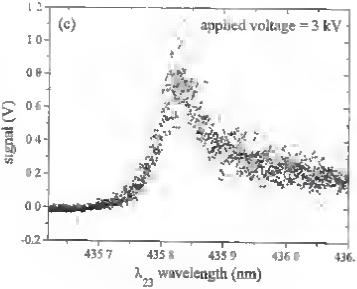

Figure 5-7 (continued)

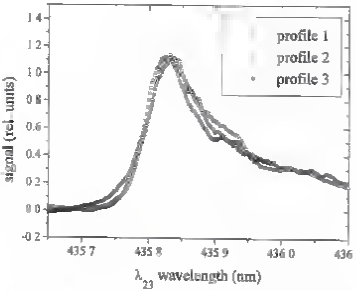

Figure 5-8 Smoothed and normalized spectral profiles of Fig 5-7

ionization signals obtained with and without λ_{34} with the assumption that, when A_{31} is absent, the signal is due only to photoionization

The reported value of the cross section for photoionization (σ_{pi}) from the 7s $^3S_1$ level is 5.3×10^{-18} cm^2.[165] The wavelength for λ_{23} was 435.832 nm, which corresponds to 2.84 eV or 2.2×10^{18} photons J^{-1}. Because λ_{23} had an energy of 22 μJ and a beam diameter of 0.0312 cm^2, this corresponds to 4.84×10^{13} photons or 1.55×10^{15} photons cm^{-2}. For these measurements the pulse energy of λ_{23} was reduced to 22 μJ in order that the enhancement factor due to the addition of λ_{34} could be measured without exceeding the linear range of the preamplifier. The efficiency of photoionization from the 7s $^3S_1$ level (two-step excitation) is defined here as the product of the laser photon fluence, E_{ph} (photons cm^{-2}), at λ_{23} and the photoionization cross section, i.e

$$\eta \text{ (2-step)} = E_{ph} \times \sigma_{pi} \qquad \textbf{(5-1)}$$

The use of the above values gives an efficiency of 0.0082 (0.82%). The enhancement factor, E.F., for the three-step excitation ($n \sim 12$) over the two-step excitation was calculated as

$$E.F = \text{signal } (\lambda_1 + \lambda_2 + \lambda_3) / \text{signal } (\lambda_2 + \lambda_1) \qquad \textbf{(5-2)}$$

From the experiment, a value of 32 3 was calculated for $n = 12$ Since the spectral irradiance of both λ_{12} and λ_{23} was more than sufficient to saturate the two Hg transitions the overall ionization efficiency from $12p\ ^3P^0_2$ can be calculated as

$$\eta_{eff}(3\text{-step}) = \eta\ (2\text{-step}) \times E\ F \times \frac{g_2}{g_0 + g_1 + g_2} \qquad (5\text{-}3)$$

where g is the statistical weight of the first (g_1), second (g_2), and third (g_3) levels. In this way, η_{eff} for $n = 12$ is calculated to be 0 11 (11%). It is important to point out that further increase in the laser energy density for λ_{34} led to the appearance of a background signal due to multiphoton ionization of the buffer gas the calculated ionization efficiency of 0 11 corresponds to the best measurement with minimal background. The values calculated similarly for $n = 10$ and 11 are 0 051 and 0 055, respectively

It is now possible to estimate a limit of detection (LOD) for $n = 12$ with avalanche amplification of the signal. The preamplifier used in this study was previously calibrated and produced 0 15 μV per electron [187] The amplifier-noise limited LOD was determined to be 1500 electrons. With an avalanche amplification factor of 908 thus corresponded to 1500 e /908 or 1 65 electrons per laser pulse For $n = 12$, with an ionization efficiency of 0 11, thus corresponded to (1 65 e /pulse)/(0 11 e /atom) or about 15 atoms per pulse in the laser irradiated volume It is important to emphasize that this was for a single pulse measurement. Typical signal averaging procedures would have provided substantial S/N enhancement. While this calculation shows that our technique provides the most sensitive detection ever reported for mercury atoms in a cold environment much work is

needed to validate this result experimentally. Indeed, due to Hg contamination of the system, a background signal of approximately 10^3 - 10^4 Hg atoms in the interaction region was observed. This background could not be eliminated from our present setup.

Conclusions

It has been shown that a detection limit of several atoms in a single laser pulse can be attained for the RI detection of Hg atoms in P-10 gas at ambient temperature. This is possible due to an avalanche effect which increases the signal by nearly three orders of magnitude. Direct proportionality with the initial concentration of atoms is maintained over a large dynamic range. This avalanche effect provides a detection capability of ~1 6 e during a single laser pulse.

CHAPTER 6
METHOD OPTIMIZATION AND ANALYTICAL CONSIDERATIONS

In order to prove this method to be analytically useful for the ultratrace detection of Hg, it was necessary to improve and experimentally determine the limit of detection as well as to determine the behavior of the signal as a function of changing concentration. In order to improve the limit of detection, two options were studied: (1) increasing the avalanche amplification factor and (2) increasing the efficiency of ionization. With these improvements and the interfacing of a sample introduction system, ultratrace levels of Hg were determined from aqueous samples.

Experimental

The experimental setup is shown in Figure 6-1. Two dye lasers (laser 1: Molectron, Portland, OR; laser 2, Model Scanmate 1, Lambda Physik, Acton, MA) were pumped by an excimer laser (Model LPX-240i, Lambda Physik, Acton, MA) operated with XeCl. The excitation scheme with the wavelengths of the two dye lasers is shown in Figure 6-2. Laser dyes used include Coumarin 500 (Exciton, Dayton, OH) frequency doubled, for λ_1, and Furan 2 (Lambda Physik, Acton , MA) for λ_2. Pulse energies were typically 100-150 mJ for the excimer, 2-30 μJ for λ_1, and 150-300 μJ for λ_2.

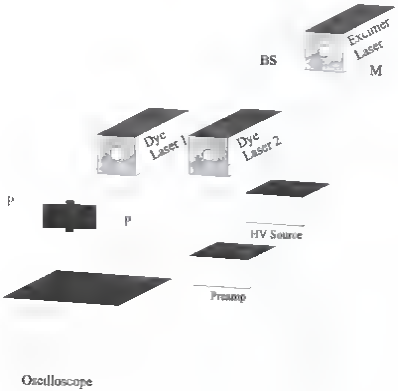

Figure 6-1 Experimental setup

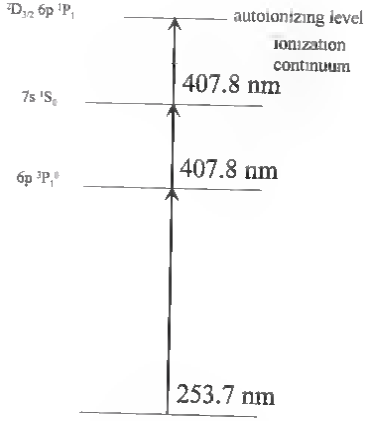

Figure 6-2 Excitation scheme for Hg

The beams were directed with prisms into the detection cell on electron counter pictured in Figure 6-3. The electron counter consisted of a stainless steel casing which housed two electrodes and Teflon insulation. The high voltage electrode was a stainless steel tube in which the collection electrode a 0.1 mm dia. W wire, was contained. The laser beams passed directly over the collection electrode *via* two holes in the casing. An inert gas stream carrying Hg atoms entered the cell directly into the tube electrode through a hole in the side of the casing and was allowed to escape through the laser beam holes.

The tube electrode was connected to a high voltage source which applied varying potentials (0-3 kV) between the electrodes. The collection electrode was connected through a charge sensitive preamplifier (Avangard Inc., Russia) to a fast digitizing oscilloscope (Model 620A, Tektronix, Beaverton OR). In addition, the amplified signal was averaged using a boxcar averager (Model SR560, Stanford Research Systems, Sunnyvale CA) and recorded on a laptop computer. In this way, the resonance ionization signal was detected and recorded.

Comparisons studies were carried out between the electron counter and the cell which was used in previous chapters, shown for the sake of clarity in Figure 6-4. The quartz cell housed two Ni planar electrodes. A high voltage was applied to one of the electrodes, and signal collection was carried out with the other electrode which was connected through the charge sensitive preamplifier to the oscilloscope. A vacuum pump and P-10 gas cylinder were connected to the cell to allow varying pressures of buffer gas into the cell. A small drop of Hg was contained in the cell.

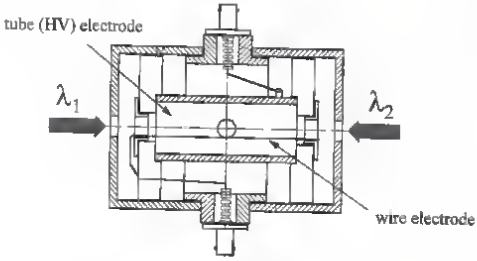

Figure 6-3 Electron counter

Figure 6-4 Quartz cell containing two planar Ni electrodes.

In order to make atomic absorption measurements for calibration, a hollow cathode lamp (Fisher Scientific) was used as the light source and a photomultiplier tube was used to detect the transmitted 253.7 nm light. The PMT was masked with a 254 nm cutoff filter and the signals were displayed on the oscilloscope.

Aqueous samples of Hg were made by diluting a 10 ppm Hg solution (SPEX Chemical, Metuchen, NJ) with 5% HCl (Optima grade, Fisher Scientific) in water (Millipore grade). A solution of $SnCl_2$ (3% $SnCl_2$, 15%HCl) was used as the reducing agent for cold vapor generation. The solution was made by dissolving the $SnCl_2$ in the acid and diluting with Millipore water. As any Hg contained in the solution became reduced, the solution was then purged with Ar gas for several hours to remove any free Hg from the solution. A solution of 2 M HCl was made up to further dilute the Hg solutions for cold vapor generation.

The apparatus used for the cold vapor generation sample introduction is shown in Figure 6-5. A glass cylinder (41 mL) was used to hold the solution, which consisted of 10 mL 2 M HCl, 3 mL $SnCl_2$ solution, and varying volumes of 100 ppb Hg (1.5 - 0.1 mL, corresponding to 150 - 1 ng Hg). The $SnCl_2$ solution was added last, just prior to sealing the cell. The cell was sealed with a plastic cork, into which two holes had been drilled to allow gas to enter and exit the cell. The P-10 gas was passed into the cell via Teflon tubing and through the cell using a gas bubbler with a glass frit, which was submerged in the solution. In this way, P-10 gas was bubbled directly into the solution and free Hg was purged into the gas phase. The resulting gas stream, carrying free Hg (as well as some water vapor), was passed out of the generation system and directly into the electron counter.

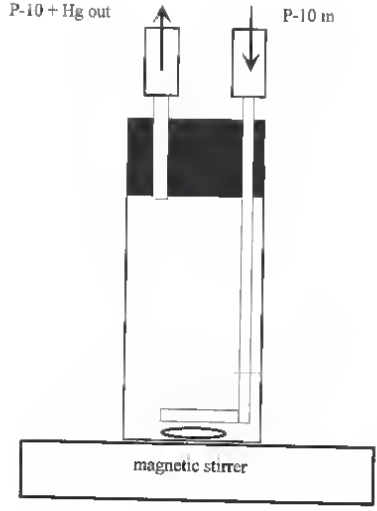

Figure 6-5 Cold vapor generation apparatus

The procedure for Hg atom generation involved pipetting the solution into the cell, sealing the cell, allowing it to mix for three minutes (using a magnetic stirrer), and then allowing the gas to bubble through the solution. With this cell, ionization signals lasted as long as 3 minutes. The high voltage applied between the electrodes was 1.94 kV, and the P-10 gas flow rate was 3.3 mL/s.

Results and Discussion

Performance of Excitation Scheme

With the excitation scheme described in previous chapters, the highest ionization efficiency achieved was 11%, which occurred with excitation of the Rydberg level corresponding to principal quantum number $n = 12$. In order to improve this efficiency, the excitation scheme was changed from one involving collisional ionization from a Rydberg level to one involving photoionization to an autoionizing level above the ionization continuum. The excitation to this type of real autoionizing level can produce a dramatic signal enhancement as compared to a photoionization scheme where an real level is reached. This scheme was first reported by Bialy *et al*.[168], who observed an increase in signal of 20 times over that with the scheme used previously in this work.

At low applied voltages (<200 V), an increase in signal of 90 times was observed with both lasers ($\lambda_1 + \lambda_2$) over the signal obtained with just λ_1. However, when higher voltages were applied (such as those necessary to obtain avalanche amplification of the signal, 1-3 kV), this enhancement factor dropped to as low as a factor of 2. In order to

ascertain the reason for this the enhancement factor ($\lambda_1 + \lambda_2$ signal/λ_1 signal) was studied as a function of pressure with the quartz cell shown in Figure 6-4

With this cell, at a P-10 gas pressure of 30 mTorr, an enhancement factor of 1400 was observed. Even at 760 Torr, an enhancement of 450 was achieved. It was clear that the decrease in the enhancement factor was not due to the signal detection occurring at atmospheric pressure in the electron counter. A possible reason for this loss, based on our previous studies, is given below

In Chapter 4, the structure of the Rydberg lines as a function of pressure and Stark effects was studied. It was observed that an increase in pressure for the higher lying lines caused some broadening in the lines while an increase in the electric field caused a large amount of broadening and splitting which increased as the lines got closer to the ionization continuum It would then be probable that autoionizing levels, which appear above the ionization continuum, could suffer the same effects. In fact, with the more different electric field configuration used in the electron counter, and with voltages of 1-3 kV applied between the electrodes, it was possible that the autoionizing level could become so broadened that it could not be excited with the available laser energy For this reason, the enhancement in signal that should occur due to the excitation of this level would be lost With this loss of enhancement, the new scheme resulted in a decrease in ionization efficiency over the previous scheme of 10^3 -10^4 times It is important to note however, that this loss of enhancement would be suffered by any excitation scheme that was affected by Stark effects including the scheme used in Chapters 3-5 This is due to the new electrode configuration used in the electron counter

Performance of Electron Counter

In order to improve the avalanche amplification factor, an electron counter was designed. The main differences between the electron counter and the cell used in Chapter 5 was the use of an enclosed inert gas stream carrying the Hg, which protected the excited Hg atoms from quenching due to collisions with air and water molecules, as well as a change in the electric field configuration due to the change in electrode design. With this new design the field is ~100 times greater at the collection electrode than it was in the previously used cell (Figure 6-4).

To calculate the avalanche amplification factor attainable with this cell, the signal was studied as a function of applied high voltage. This is shown in Figure 6-6. The behavior observed was typical of avalanche amplification. In the region from 0-200 V, an increase in signal was observed. This was not a result of an increase in the number of charges being created, but rather an increase in those actually being collected. In the region from 200-1000 V there was no increase in signal, because all of the charges were being detected but no new charges were being created. However, for applied voltages between 1-3 kV, the signal began to increase rapidly with an increasing voltage. In this region, electrons traveling to the anode to be detected were creating new charges by collisionally ionizing the buffer gas atoms in their path. The avalanche amplification factor calculated as the increase in signal between the smallest signal in which all charges are collected (at 200 V) and the largest avalanche signal attained (at 3 kV) was found to be 6.6×10^5. The amplification of the non-selective signal was observed by measuring the signal with only λ_1, detuned from the 253.7 nm resonance transition, and

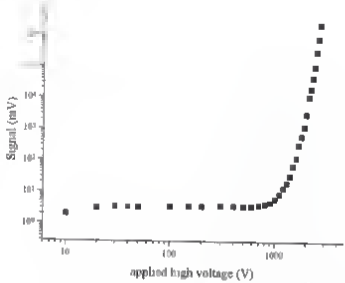

Figure 6-6 Avalanche amplification of RI signal

the signal with only λ_2. At an applied high voltage of 200 V no signal was observed for either case. At an applied voltage of 2.7 kV the signal from λ_1 (detuned) was 25.6 mV, from λ_2, it was 104.4 mV giving a combined background of 130 mV. This background signal was subtracted from each value in Figure 6.6. The electron counter resulted in a huge improvement over the previous cell, with which an avalanche amplification factor of 908 was observed.

It was then necessary to show that this avalanche amplification signal was proportional to the number of charges originally created in the laser volume. This was done in the same manner as in Chapter 5, by spectrally scanning the second laser step and comparing the spectra observed for HV = 200 V and 2.7 kV. The results are shown in Figure 6-7. The solid line represents the avalanche amplification signal (smoothed), while the dotted line is the spectral scan (smoothed) obtained from just the number of charges created as a result of ionized Hg. This signal was actually much smaller than the avalanche signal, but was normalized in Fig. 6-7 to the same size. It was concluded that the behavior of the signal was the same in both cases. It was therefore clear that the avalanche amplification signal was proportional to the original number of charges created in the laser volume.

Limit of Detection

Using the electron counter, the limit of detection was determined. This was done by correlating the resonance ionization signals to atomic absorption measurements. The cross-section of atomic absorption was calculated after making absorption measurements

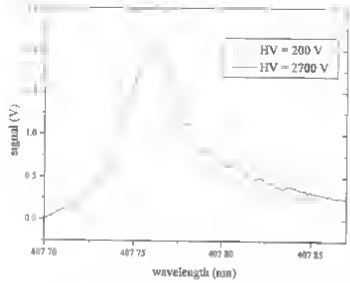

Figure 6-7 Spectral profiles of λ_2^-

with a Hg reference cell with a pathlength of 1 65 mm. The absorption fraction for this cell was observed to be 0 35 At atmospheric pressure, the number density in the cell was ~4 0 x 10^{13} atoms cm^{-3} The cross section of absorption is then calculated as

$$\sigma_A = 0.46/(4.0 \times 10^{13} \text{ atoms cm}^{-3})(0.165 \text{ cm}) \qquad \textbf{(6-1)}$$

which gives a value of 7 0 x 10^{-14} cm^2

The linearity of the electron counter for Hg in the gas stream was determined by correlating absorption signals at different gas flow rates with the ionization signals at these rates. It was observed that at higher flow rates the signal decreased because the residence time of the Hg between the electrodes was decreased Three flow rates were used and both the absorption and ionization signals measured. The ionization signals were measured without the preamplifier as the concentrations observable with AA were large enough to be observed without it. The number of Hg atoms was calculated from the absorption signal using equation 6-1 these results are shown in Figure 6-8

The absorption fraction through the electron counter (which had a pathlength of 10 cm) was observed to be 0 0056 for the highest buffer gas flow rate at which the absorption signal could still be measured. Therefore, the number density of Hg atoms in the cell is calculated as

$$n = 0.0024/(7.0 \times 10^{-14} \text{ cm}^2)(10 \text{ cm}) \qquad \textbf{(6-2)}$$

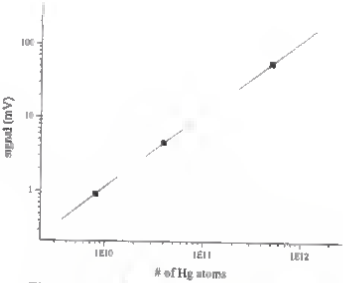

Figure 6-8 Calibration curve of Hg atoms in the gas phase, correlated with atomic absorption measurements.

which gives a value of 3.4×10^9 atoms cm^{-3}. The resonance ionization signal for this same concentration had a signal to-noise ratio of 1840 (with only λ_1 used for excitation). Therefore, the smallest number density which can be detected with this method is

$$3.4 \times 10^9 \text{ atoms cm}^{-3}/1840 = 1.9 \times 10^6 \text{ atoms cm}^{-3} \qquad \textbf{(6-3)}$$

which corresponds to 1.9×10^3 atoms in the measurement (laser irradiated) volume (0.1 $cm^2 \times 10$ cm). It is believed that this is limited by the poor degree of ionization efficiency.

Analytical Curve

Preliminary studies were carried out using the cold vapor generation sample introduction procedure for varying amounts of Hg vapor. The analytical curve for the technique is shown in Figure 6-9. The curve ranges from the highest concentration detectable at this high voltage (1.94 kV), which is determined by the saturation level of the preamplifier to the lowest concentration, which is limited by the blank. However, different ranges of Hg can be detected by changing the high voltage applied to the cell. As evidenced in Figure 6-6, an increase in applied voltage can greatly increase the signal. In this way, higher concentrations can be detected by decreasing the applied voltage, while smaller concentrations can have their signals increased by increasing the applied voltage.

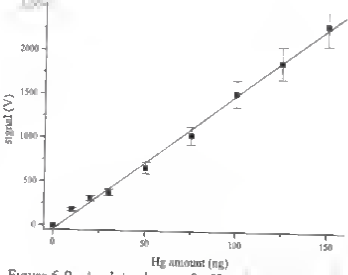

Figure 6-9. Analytical curve for Hg with CV generation from aqueous solutions

Improvements on this method include removing water vapor from the stream going into the electron counter. This water can cause quenching of the excited Hg state, decreasing the ionization efficiency. This can be carried out by inserting a drying tube, containing magnesium perchlorate or some other drying agent, into the tubing which carries the Hg to the electron counter. This will not only increase the ionization efficiency but will also decrease the part of the blank signal which may be due to nonselective ionization of the water vapor. In addition, attempts may be made to decrease the amount of Hg present in the blank signal.

Conclusions

With the electron counter as the detection cell, the avalanche amplification factor was increased to 6.6×10^5, giving a larger signal. However, the number of electrons originally created in the laser volume was decreased by a factor of between 10^3 - 10^4 by using the new excitation scheme. It is believed that the electric field configuration used in the electron counter had a large broadening effect on the autoionizing level employed in this excitation scheme. However, even with a low ionization efficiency, a detection limit of 1.9×10^5 atoms (63 ag) in the measurement volume was achieved.

Preliminary studies of the signal as a function of Hg concentration in solution using the cold vapor generation method for sample introduction indicated linearity over a wide range of Hg quantities. The lowest level measured, 10 ng, was blank limited due to Hg and other impurities. With removal of these impurities, the use of an optimal excitation/ionization scheme, an optimized mercury generation scheme involving

removal of water and an optimized ionization detector the detection should be lowered by 10^6 - 10^{12} orders of magnitude based upon the earlier studies in this dissertation.

CHAPTER 7
CONCLUSIONS AND FUTURE WORK

In this work, a technique for the ultratrace detection of Hg using resonance ionization spectroscopy has been developed. After carrying out fundamental studies of the resonance ionization of Hg, a detection scheme was chosen and optimization of the scheme was carried out. A detection limit of 2.5×10^6 atoms cm^{-3} (0.83 fg cm^{-3}) in a pure P-10 gas stream was achieved. In addition, a sample introduction method involving the cold vapor generation of Hg atoms from solution was developed and interfaced to the resonance ionization electron counter. A theoretical detection limit of 15 atoms was calculated for RIS of Hg.

Future work on this project should include increasing the ionization efficiency of Hg by optimizing the choice of excitation scheme. This scheme should include the use of an excited Hg level which is not very susceptible to Stark effects at high applied voltages.

In addition, the sample introduction system for solutions should be improved in order to take full advantage of the sensitivity of which this method is capable. This would involve removing water vapor from the inert gas stream before it enters the electron counter, where water vapor can cause quenching of the excited Hg. The method should also be applied to air samples, where it may prove to be most useful.

Other future projects could include interfacing the electron counter to gas chromatography which would allow speciation of the different forms of mercury including the highly toxic methyl mercury

This method could also be applied to different elements by using a hydride generation sample introduction method. Any element that can be vaporized without the use of heat can then be studied using the avalanche amplification of the RIS signal In addition the method could be amenable to volatile molecules.

LIST OF REFERENCES

1 Barbosa, A.C., Bonschio, A.A. East, G.A. Ferrari, I. Goncalves, A. Silva, P.R.M., da Cruz, T.M.E. *Water Air and Soil Pollut* **1995**, *80*, 109

2 Homewood, B. *New Sci* **1991**, Nov 9, 18

3 Glass, G.E., Sorensen, J.A., Schmidt, K.W., Rapp, G.R. *Environ. Sci. Technol* **1990**, *24*, 1059

4 Glass, G.E., Sorenson, J.A., Schmidt, K.W., Rapp, G.R., Yap, D., Fraser, D. *Water Air and Soil Pollut* **1995**, *80*, 235

5 Fleming, L.E., Watkins, S., Kaderman, R., Levin, B., Ayyar, D.R., Buzzio, M., Stephens, D., Bean, J.A. *Water Air and Soil Pollut* **1995**, *80*, 41

6 Rood, B.E., Gottgens, J.F., Delfino, J.J., Earle, C.D., Crisman, T.L. *Water Air and Soil Pollut* **1995**, *80*, 981

7 Woodson, T.T. *Rev. Sci. Instrum.* **1939**, *10*, 308

8 Chilov, S. *Talanta*, **1975**, *22*, 205

9 Analytical Methods Committee, Society for Analytical Chemistry *Analyst* **1965**, *90*, 515

10 Ure, A.M. *Anal. Chim. Acta* **1975**, *76*, 1

11 Morita, H., Tanaka, H., Shimomura, S. *Spectrochim. Acta Part B*, **1995**, *50*, 69

12 Muscat, V.L., Vickers, T.J., Andren, A. *Anal. Chem.*, **1972**, *44*, 218

13 Jensen, S., Jernelov, A. *Nature*, **1968**, *223*, 753

14 Wood, J.M., Kennedy, F.S., Rosen, C.G. *Nature*, **1968**, *220*, 173

15 Rapsomanikis, S., Weber, J.H., in *Organometallic Compounds in the Environment*, P.J. Craig, Ed., Wiley, New York, 1986, p. 279

16 Hatch, W.R., Ott, W.L. *Anal. Chem.*, **1968**, *40*, 2085

1 Gilbert, T.R., Hume, D.N. *Anal. Chim. Acta*, **1973**, *65*, 461

18 Zhou, C.Y., Wong, M.K., Koh, L.L., Wee, Y.C. *Anal. Sci.* **1996**, *12*, 47

19 Toffaletti, J., Savory, J. *Anal. Chem.* **1975**, *47*, 2091

20 Rooney, R.C. *Analyst* **1976**, *101*, 678

21 Yamamoto, Y., Kumamaru, T., Shiraki, A. *Fresenius Z. Anal. Chem.*, **1978**, *292*, 273

22 Welz, B., Schubert-Jacobs, M. *Fresenius Z. Anal. Chem.*, **1988**, *331*, 324

23 Brindle, I.D., Zhang, S. *Spectrochim. Acta Part B*, **1996**, *51*, 1777

24 Tong, S. *Anal. Chem.*, **1978**, *50*, 412

25 Oda, C.E., Ingle, J.D. Jr. *Anal. Chem.*, **1981**, *53*, 2030

26 Goto, M., Shibakawa, T., Arita, T., Ishii, D. *Anal. Chim. Acta*, **1982**, *140*, 179

27 Colina de Vargas, M., Romero, R.A. *At. Spectrosc.*, **1989**, *10*, 160

28 Yamada, E., Yamada, T., Sato, M. *Anal. Sci.*, **1992**, *8*, 863

29 Saraswati, R., Beck, C.M., Epstein, M.S. *Talanta*, **1993**, *40*, 1477

30 Hanna, C.P., McIntosh, S.A. *At. Spectrosc.*, **1995**, *16*, 106

31 Murphy, J., Jones, P., Hill, S.J. *Spectrochim. Acta Part B*, **1996**, *51*, 1867

32. Dumarey, R., Heindrickx, R., Dams, R., Hoste, J. *Anal. Chim. Acta*, **1979**, *107*, 159

33 Dumarey, R., Dams, R., Hoste, J. *Anal. Chem.*, **1985**, *57*, 2638

34 Yoshida, Z., Motojima, K. *Anal. Chim. Acta*, **1979**, *106*, 405

35 Fitzgerald, W.F., Gill, G.A. *Anal. Chem.*, **1979**, *51*, 1714

36 Ólafsson, J. *Anal. Chim. Acta*, **1974**, *68*, 207

37 Freimann, P., Schmidt, D. *Fresenius Z. Anal. Chem.*, **1982**, *313*, 200

38 Welz, B., Melcher, M., Sinemus, H.S., Mauer, D. *At. Spectrosc.*, **1984**, *5*, 37

39 Temmerman, E. Dumarey R. Dams R *Anal Lett* **1985** *18* 203

40 Gill G.A. Fitzgerald W F *Mar Chem* **1987** *20* 227

41 Welz, B Tsalev D , Sperling, M *Anal Chim Acta*, **1992**, *261*, 91

42 Hanna, C.P. Tyson, J.F. McIntosh S *Anal Chem* **1993**, *65* 653

43 McIntosh, S *At Spectrosc* ,**1993** *14*, 47

44 Streško V , Polakovičová, I , Kubova, J *J Anal At Spectr* **1994** *9* 1173

45 Garcia, M F Garcia, R.P., Garcia, N B Sanz-Medel, A *Talanta* **1994** *41*, 1833

46 Matsunaga, K., Takahashi S *Anal. Chim. Acta*, **1976**, *87*, 487

47 Dumarey, R. Heindrickx R., Dams, R. *Anal Chim. Acta*, **1980**, *116*, 381

48 Vanmeir G , Vandecasteele C , Temmerman, E., Dams, R., Verscheck, J *Mikrochim Acta*, **1988** *111*, 305

49 Horvat, M., Lopéna, V Pihlar B *Anal Chim Acta*. **1991** *243*, 71

50 Brandvold, D.K , Martinez, P Matlock, C *Anal Instr* **1993** *21*, 63

51 Ombaba, J.M *Microchem J*, **1996** *53*, 195

52 Ellis, L.A., Roberts, D J *J Anal At Spectrom* **1996** *11*, 1063

53 Keller, B.J. Peden M E Rationetti A *Anal Chem* **1984** *56* 2617

54 Hladky, Z. Ršova, J , Fišera, M *J Anal At Spectr* , **1996**, *5*, 691

55 Lee, S H. Jung, K H., Lee, D S *Talanta*, **1989** *36*, 999

56 Siemer D D , Hageman, L *Anal Chem* , **1980**, *52* 105

57 Baxter D C Frech, W *Anal. Chim. Acta* **1989** *225*, 175

58 Rapsomanikis, S , Craig, P.J *Anal Chim Acta*, **1991** *248*, 563

59 Fischer R. Rapsomanikis, S Andreae M O *Anal Chem* , **1993** *65*, 763

60 Emteborg, H., Sinemus, H.W., Radziuk, B., Baxter, D.C., Frech, W. *Spectrochim. Acta, Part B* **1996**, *51*, 829.

61 Ahmed, R., Mavi, K., Stoeppler, M. *Fresenius Z. Anal. Chem.* **1987**, *326*, 510.

62 Sarzanini, C., Sacchero, G., Aceto, M., Abollino, O., Mentasti, E. *Anal. Chim. Acta* **1994**, *284*, 661.

63 Fujita, M., Takahatake, E. *Anal. Chem.* **1983**, *55*, 454.

64 Azpun, B., Fernandez, M.L., Blanco, E., Sanz-Medel, A. *J. Anal. At. Spectr.* **1994**, *9*, 1279.

65 Madrid, Y., Cabrera, C., Perez-Corona, T., Camara, C. *Anal. Chem.* **1995**, *67*, 750.

66 Winefordner, J.D., Staab, R.A. *Anal. Chem.*, **1964**, *36*, 165.

67 Hutton, R.C., Preston, B. *Analyst*, **1980**, *105*, 981.

68 Morita, H., Kimoto, T., Shimomura, S. *Anal. Lett.*, **1983**, *16*, 1187.

69 Swift, R.P., Campbell, J.E. *Spectroscopy*, **1993**, *8*, 38.

70 Lamble, K.J., Hill, S.J. *J. Anal. At. Spectr.*, **1996**, *11*, 1099.

71 Stockwell, P.B., Corns, W.T. *Analyst*, **1994**, *119*, 1641.

72 Janjić, J., Kiurski, J. *Water Res.*, **1994**, *28*, 233.

73 Corns, W.T., Stockwell, P.B., Jameel, M. *Analyst*, **1994**, *119*, 2481.

74 Bloxham, M.J., Hill, S.J., Worsfold, P.J. *J. Anal. At. Spectr.*, **1996**, *11*, 511.

75 Muscat, V.J., Vickers, T.J., Andren, A. *Anal. Chem.*, **1972**, *44*, 218.

76 Ferrara, R., Serritu, A., Barghigiani, C., Petrosino, A. *Anal. Chim. Acta*, **1980**, *117*, 391.

77 Chan, C.C.Y., Sadana, R.S. *Anal. Chim. Acta*, **1993**, *282*, 109.

78 Cossa, D., Sanjuan, J., Cloud, J., Stockwell, P.B., Corns, W.T. *J. Anal. At. Spectr.*, **1995**, *10*, 287.

79 Cossa, D., Sanjuan, J., Cloud, J., Stockwell, P.B., Corns, W.T. *Water, Air, and Soil Pollut.*, **1995**, *80*, 1279.

80 Poissant, L., Harvey, B., Castmir, A. *Env. Technol.* **1996**, *17*, 891.

81 Rosta, W., Badini, R.G., Smith, B.W., Stevenson, C.L., Winefordner, J.D. *Spectrochim. Acta Part B* **1993**, *48*, 627.

82 Pagano, S.T., Smith, B.W., Winefordner, J.D. *Talanta* **1994**, *41*, 2073.

83 Lancioni, R.L., Drew, D.M. *Spectrochim. Acta Part B*, **1985**, *40*, 107.

84 Bloom, N., Fitzgerald, W.F. *Anal. Chim. Acta.*, **1988**, *208*, 151.

85 Saouter, E., Blattmann, B. *Anal. Chem.*, **1994**, *66*, 2031.

86 Jones, R.D., Jacobson, M.E., Jaffe, R., West-Thomas, J., Arfstrom, C., Alh, A. *Water, Air, and Soil Pollut.*, **1995**, *80*, 1285.

87 Jean, W., McLeod, C.W. *Talanta*, **1992**, *39*, 1537.

88 Camuna-Aguilar, J.F., Pereiro-Garcia, R., Sánchez-Uria, J.E., Sanz-Medel, A. *Spectrochim. Acta Part B*, **1994**, *49*, 475.

89 Tanabe, K., Chiba, K., Haraguchi, H., Fuwa, K. *Anal. Chem.*, **1981**, *53*, 1450.

90 Nojiri, Y., Otsuki, A., Fuwa, K. *Anal. Chem.*, **1986**, *58*, 544.

91 Natarajan, S. *At. Spectrosc.*, **1988**, *9*, 59.

92. Quimby, B.D., Sullivan, J.J. *Anal. Chem.*, **1990**, *62*, 1027.

93 Tao, H., Miyazaki, A. *Anal. Sci.*, **1991**, *7*, 55.

94 Siamens, V., Harju, T., Lattinen, T., Lanjava, K., Broekaert, J.A.C. *Fresenius J. Anal. Chem.* **1995**, *351*, 11.

95. Nakahara, T., Wasa, T. *Bull. Chem. Soc. Jpn.* **1992**, *65*, 1165.

96 Cañada-Rudner, P., Garcia de Torres, A., Cano Pavón, J.M. *J. Anal. At. Spectr.* **1993**, *8*, 705.

97 Canada-Rudner, P., Cano Pavón, J.M., Garcia de Torres, A., Sanchez-Rojas, F. *Fresenius J. Anal. Chem.*, **1995**, *352*, 615.

98 Anderson, K.A., Isaacs, B., Tracy, M., Möller, G. *J. AOAC Int.*, **1994**, *77*, 473.

99 Jamoussi B , Zafiouf, M , Hassine B.B *Int J Environ. Anal Chem* **1995** *61* 249

100 Carlos de Andrade J , Bueno, M I M S *Spectrochim Acta Part B* **1994** *49* 787

101 Wrembel, H *Z Spectrochim. Acta Part B*, **1986** *41*, 247

102. Decadt, G , Baeyens, W , Bradley, D , Goeyens L *Anal Chem.*, **1985** *57*, 2788

103 Lansens, P , Meulman, C., Leermakers, M , Baeyens, W *Anal. Chim. Acta* **1990**, *234*, 417

104 Emteborg, H , Baxter D C., Sharp, M , Frech, W *Analyst* **1995** *120*, 69

105 Ceulemans, M , Adams, F C *J Anal At Spectr.*, **1996** *11*, 201

106 Costanzo, R.B , Barry, E F *Anal Chem.*, **1988** *60*, 826

107 Krull, I S , Bushee, D S , Schleicher, R.G., Smith S.B Jr *Analyst*, **1986** *111*, 345

108 Costa-Fernandez, J M., Lunzer, F , Pereiro-Garcia, R., Sanz-Medel, A *J Anal. At. Spectr* , **1995**, *10*, 1019

109 Patterson, J.E. *Anal Chim. Acta* **1984** *164*, 119

110 Chen, N , Guo, R., Lu, E P C. *Anal Chem* , **1988**, *60*, 2435

111. Chen, N., Lu, E P C *Talanta*, **1989** *36*, 479

112 Dodge W B.III, Allen, R.O *Anal Chem.*, **1981**, *53*, 1279

113 Stephens, R. *Anal Chim Acta*, **1978** *98*, 291

114 D'Silva, A , Fassel, V.A *Anal Chem.*, **1972**, *44*, 2115

115 Bhat, C.K , Bhat, C.L , Lodhi, G S , Kaul, D.K. *Environ Monit. and Assess* **1996** *41*, 77

116 Holynska, B , Ostachowicz, B , Węgrzynek, D *Spectrochim Acta Part B*, **1996**, *51* 769

117 Robert, J M , Rabenstein, D L. *Anal. Chem* , **1991** *63*, 2674

118 Lazzari, C , De Rosa, M , Rastelli, S., Cluzet, A , Palleschi V , Salvetti, A. *Laser Part Beams* **1994** *12*, 525

119 Baxter D C., Nichol R., Littlejohn D *Spectrochim Acta Part B* **1992**, *47* 1155

120 Haraldsson C., Westerlund, S., Öhman P *Anal Chim Acta* **1989** *221*, 77

121 Powell M J., Quan, E S.K., Boomer D W., Wiederin, D R. *Anal Chem*, **1992**, *64* 2253

122. Brown, R., Gray D J., Tye, D *Water Air and Soil Pollut*, **1995** *80* 1237

123. Debrah, E., Denoyer, E R., Tyson, J.F *J Anal At Spectr*, **1996**, *11* 127

124 Smith R.G *Anal Chem* **1993**, *65*, 2485

125 Beauchemin, D., Siu, K.W M., Berman, S S *Anal Chem* **1988** *60* 2587

126. Hintelmann, H., Evans, R.D., Villeneuve J V *J Anal At Spectr* **1995** *10* 619

127 Bushee, D S *Analyst* **1988** *113*, 1167

128 Shum, S C.K., Pang, H., Houk, R.S *Anal Chem.*, **1992** *64*, 2444

129 Huang, C., Jiang, S *J Anal At Spectr*, **1993** *8*, 681

130 Bloxham, M.J., Gachanja, A., Hill, S.J., Worsfold, P.J *J Anal. At Spectr*, **1996** *11*, 145

131 Abbas, M N., EL-Assy, N B., Abdel-Moniam, SH *Anal Lett.* **1989** *22* 2575

132. Singh, H B., Kumar, B., Sharma, R.L., Katyal, M. *Analyst* **1989** *114*, 853

133 Ramesh, A. *Analyst*, **1993** *118*, 945

134 Shekhovtsova, T.N., Chernetskaya, S V *Anal Lett*, **1994** *27*, 2883

135 Shekhovtsova, T N., Chernetskaya, S V., Dolmanova, I F *J Anal. Chem.*, **1995**, *50*, 280

136 Jiang, W., Zhu, Y., Jin, G., Wu, G *Anal. Lett*, **1996** *29*, 2221

137 Holzbecher J., Ryan, D.E *Anal. Chim. Acta*, **1973**, *64*, 333

138 Narinesingh, D., Mungal, R., Ngo, T T *Anal Chim Acta*, **1994** *292* 185

139 Douglas, J *EPRI J*., **1991**, Dec., 4

140 Hurst, G S Payne M G Editors *Principles and Applications of Resonance Ionization Spectroscopy* IOP Publishing LTD Bristol, 1988

141 Letokhov V S *Laser Photoionization Spectroscopy* Academic Press Inc., Orlando FL 1987

142 J C Travis J C and Turk G C Editors *Laser Enhanced Ionization Spectroscopy* Wiley Series on Chemical Analysis Winefordner J D Ed., Vol 136 Wiley, New York 1996

143 Hurst, G S , Nayfeh M.H., Young J P *Appl Phys Lett.*, **1977**, *30*, 229

144 Muzolek, A W *Anal Chem.* **1981**, *53*, 118.

145 Dyer P Baldwin, G C., Kittrell, C Imre, D G Abramson, E *Appl Phys Lett.*, **1983** *42*, 311

146 Normand, D , Morellec J., Reif J *J Phys B. At Mol Phys* , **1983** *16*, L227

147 Bushaw B.A *Anal Chem* **1985** *57*, 2397

148 van de Weijer, P Cremers R.M.M *Opt Comm* , **1985** *54*, 273

149 Kramer J *J Appl Phys* , **1988** *64*, 1758

150 Matveev, O I , Smith, B W Omenetto, N , Winefordner, J D *Spectrochim. Acta Part B* **1996** *51* 563

151 Marunkev, A G Chekalin, N V *Opt Spectrosc (USSR)*, **1986**, *61* 461

152 Axner, D , Berglind, T *Appl Spectrosc.*, **1989**, *43*, 940

153 Omenetto, N Smith, B W Farnsworth, P B Winefordner, J D *J Anal. At. Spectrom.*, **1992**, *7*, 89

154 Vlasov, I.I., Chekalin N.V *Spectrochim Acta Part B* **1993**, *48*, 597

155 Niemax K *Appl Phys B* **1983** *32*, 59

156 Matveev, O.I., Omenetto, N *Spectrochim. Acta Part B*, **1994** *49* 691

157 Broglia, M Catemi, F , Montone A Zampetti, P *Phys Rev A*, **1987** *36* 705

158 Berthaud, T Lipinsky, J , Camus P , Stelhe' J.L *Anal Chem* **1983** *55* 960

159 Havrilla, G., Schenck, P.K., Travis, J.C., Turk, G.C. *Anal. Chem.* **1984**, *56*, 186

160 Magnusson, I. *Spectrochim. Acta Part B.* **1987**, *42*, 1113

161 Matveev, O.I., Ph.D. Dissertation, Moscow State University, Moscow (Russ.) **1979**

162. Matveev, O.I., Cavalli, P., Omenetto, N. *AIP Conference Proceedings (RIS-94 Bernkastel Kues, Germany)*, **1994**, *329*, 269

163 Moore, C.E., "Atomic Energy Levels, Volume 3," NSRDS-NBS 35, Dec. 1958

164 Boudreau, D., Ljungberg, P., Axner, O. *Spectrochim. Acta Part B*, **1996**, *51*, 413

165 Saloman, E.B. *Spectrochim. Acta Part B*, **1991**, *46*, 367

166 Gallagher, T.F., "Rydberg Atoms" University Press, Cambridge 1994

167. Axner, O., Berglind, T. *Appl. Spectrosc.*, **1986**, *40*, 1224

168 Zhang, S., Qiu, J.Z., Wang, G. *J. Quant. Spectrosc. Radiat. Transfer*, **1989**, *42*, 19

169. van Leeuwen, K.A.H., Hogervorst, W. *J. Phys. B: At. Mol. Phys.*, **1983**, *16*, 3873

170 Xu, L., Zhun, Y., Zhang, M., He, M., Want, G., Wang, Z. *Opt. Comm.*, **1991**, *82*, 12

171 König, A., Neukammer, J., Hieronymus, H., Rinneberg, H. *Phys. Rev. A*, **1991**, *43*, 2402

172. Ch'en, S., Takeo, M. *Rev. Mod. Phys.*, **1957**, *29*, 20

173 Amaldi, E., Segre, E. *Nuovo Cimento*, **1934**, *11*, 145

174 Brillet, W.L., Gallagher, A. *Phys. Rev. A*, **1988**, *32*, 1012

175 Mossberg, T., Flusberg, A., Kachru, R., Hartmann, S.R. *Phys. Rev. Lett.*, **1977**, *39*, 1523

176 Baig, M.A. *J. Phys. B: At. Mol. Phys.*, **1983**, *16*, 1511

177 Matveev, O.I. *J. Anal. Chem. (Russ.)*, **1987**, *42*, 1412

178 Matveev O I *J Anal Chem (Russ)*, **1988**, *43* 1184

179 Matveev O I Omenetto N *AIP Conference Proceedings No 329 (RIS 94)* **1994** 515

180 Turk, G C , in *Laser Enhanced Ionization Spectroscopy*, Travis J C , Turk, G C Eds , Wiley Series on Chemical Analysis, Winefordner, J D , Ed., Vol. 136 Wiley New York, 1996 pp 161-212

181 Dědina, J , Tsalev D L *Hydride Generation Atomic Absorption Spectrometry*, Wiley Chichester 1995

182. Gornushkin, I, Clara, M., Smith, B W , Niessner, R., Winefordner, J.D., in preparation for publication

183 Harrison, W W Hang, W *Fresenius J Anal Chem.*, **1996** *355*, 803-7

184 Axner, O Rubinzstein-Dunlop, H in *Laser Enhanced Ionization Spectroscopy*, Travis, J C , Turk, G C., Eds., Wiley Series on Chemical Analysis Winefordner J D , Ed., Vol. 136, Wiley, New York, 1996, pp 1-98

185 Blum, W , Rolandi L. *Particle Detection with Drift Chambers*; Springer-Verlag, New York, 1994

186 Rossi, B B Staub, H H *Ionization Chambers and Counters*, McGraw Hill, New York, 1949

187 Riter K L Clevenger W L Mordoh, L S , Matveev O.I ; Smith B W Winefordner J D *J Anal At Spectr* 1996 11, 393

188 Bishg, P. Weitkamp, C , Zobel H *AIP Conference Proceedings No 388 (Resonance Ionization Spectroscopy 1996)* American Institute of Physics, Woodbury, NY 1997

BIOGRAPHICAL SKETCH

Wendy Leigh Clevenger was born on July 12, 1970, in Albany, GA to Jerry Anderson and Linda Wooten Clevenger. She has one brother, Chuck, and one sister, Christy, and was raised in Cleveland, TN, and Spartanburg, SC. She graduated from Cleveland High School in 1988 and was named a National Merit Scholar. She then spent two years at Furman University and transferred to the University of Tennessee at Chattanooga, where she earned a Bachelor of Science degree in 1993. From there, she entered the University of Florida and joined Professor James Winefordner's research group to work on her doctoral degree in analytical chemistry.

I certify that I have read this study and that in my opinion it conforms to acceptable standards of scholarly presentation and is fully adequate, in scope and quality, as a dissertation for the degree of Doctor of Philosophy

James D. Winefordner, Chairman
Graduate Research Professor of Chemistry

I certify that I have read this study and that in my opinion it conforms to acceptable standards of scholarly presentation and is fully adequate, in scope and quality as a dissertation for the degree of Doctor of Philosophy

James A. Deyrup
Professor of Chemistry

I certify that I have read this study and that in my opinion it conforms to acceptable standards of scholarly presentation and is fully adequate, in scope and quality, as a dissertation for the degree of Doctor of Philosophy

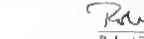

Robert T. Kennedy
Associate Professor of Chemistry

I certify that I have read this study and that in my opinion it conforms to acceptable standards of scholarly presentation and is fully adequate, in scope and quality, as a dissertation for the degree of Doctor of Philosophy

Richard A. Yost
Professor of Chemistry

I certify that I have read this study and that in my opinion it conforms to acceptable standards of scholarly presentation and is fully adequate, in scope and quality, as a dissertation for the degree of Doctor of Philosophy

Joseph J Delfino
Professor of Environmental
Engineering Sciences

This dissertation was submitted to the Graduate Faculty of Department of Chemistry in the College of Liberal Arts and Sciences and to the Graduate School and was accepted as partial fulfillment of the requirements for the degree of Doctor of Philosophy

August 1997

Dean, Graduate School